applied sciences

MDPI

Article

Exploring Methane Emission Drivers in Wetlands: The Cases of Massaciuccoli and Porta Lakes (Northern Tuscany, Italy)

Stefania Venturi [1,2,*], Franco Tassi [1,2], Jacopo Cabassi [2], Antonio Randazzo [1,2], Marta Lazzaroni [1,2], Francesco Capecchiacci [1,2,3], Barbara Vietina [4] and Orlando Vaselli [1,2]

1 Department of Earth Sciences, University of Florence, Via G. La Pira 4, 50121 Firenze, Italy; franco.tassi@unifi.it (F.T.); antonio.randazzo@unifi.it (A.R.); marta.lazzaroni@unifi.it (M.L.); francesco.capecchiacci@unifi.it (F.C.); orlando.vaselli@unifi.it (O.V.)
2 Institute of Geosciences and Earth Resources (IGG), National Research Council of Italy (CNR), Via G. La Pira 4, 50121 Firenze, Italy; jacopo.cabassi@igg.cnr.it
3 Istituto Nazionale di Geofisica e Vulcanologia (INGV), Sezione di Napoli, Osservatorio Vesuviano, Via Diocleziano 328, 80125 Napoli, Italy
4 Environment Office, Municipality of Montignoso, Via Fondaccio 11, 54038 Montignoso (MS), Italy; barbara.vietina@comune.montignoso.ms.it
* Correspondence: stefania.venturi@unifi.it

Abstract: Wetlands are hotspots of CH_4 emissions to the atmosphere, mainly sustained by microbial decomposition of organic matter in anoxic sediments. Several knowledge gaps exist on how environmental drivers shape CH_4 emissions from these ecosystems, posing challenges in upscaling efforts to estimate global emissions from waterbodies. In this work, CH_4 and CO_2 diffusive fluxes, along with chemical and isotopic composition of dissolved ionic and gaseous species, were determined from two wetlands of Tuscany (Italy): (i) Porta Lake, a small wetland largely invaded by *Phragmites australis* reeds experiencing reed die-back syndrome, and (ii) Massaciuccoli Lake, a wide marsh area including open-water basins and channels affected by seawater intrusion and eutrophication. Both wetlands were recognized as net sources of CH_4 to the atmosphere. Our data show that the magnitude of CH_4 diffusive emission was controlled by CH_4 production and consumption rates, being mostly governed by (i) water temperature and availability of labile carbon substrates and (ii) water column depth, wind exposure and dissolved O_2 contents, respectively. This evidence suggests that the highest CH_4 diffusive fluxes were sustained by reed beds, providing a large availability of organic matter supporting acetoclastic methanogenesis, with relevant implications for global carbon budget and future climate models.

Keywords: wetlands; CH_4; diffusive flux; carbon budget; greenhouse gases; macrophytes; RDBS; surface waters

check for updates

Citation: Venturi, S.; Tassi, F.; Cabassi, J.; Randazzo, A.; Lazzaroni, M.; Capecchiacci, F.; Vietina, B.; Vaselli, O. Exploring Methane Emission Drivers in Wetlands: The Cases of Massaciuccoli and Porta Lakes (Northern Tuscany, Italy). *Appl. Sci.* **2021**, *11*, 12156. https://doi.org/10.3390/app112412156

Academic Editors: Gianluca Bianchini and Claudio Natali

Received: 13 November 2021
Accepted: 15 December 2021
Published: 20 December 2021

Publisher's Note: MDPI stays neutral with regard to jurisdictional claims in published maps and institutional affiliations.

Copyright: © 2021 by the authors. Licensee MDPI, Basel, Switzerland. This article is an open access article distributed under the terms and conditions of the Creative Commons Attribution (CC BY) license (https://creativecommons.org/licenses/by/4.0/).

1. Introduction

Surface aquatic systems only cover a small fraction of global land surface [1,2]. Nevertheless, they play a crucial role in the global carbon cycle, as they regulate the transport of terrestrial carbon between lands and seas. Accordingly, attention is increasingly being devoted to studying the contribution of water reservoirs to climate change and understanding feedback mechanisms related to global warming of aquatic ecosystems, e.g., [3,4]. Among surface aquatic systems, wetlands are highly productive ecosystems capable of sequestering large amounts of carbon from the atmosphere through photosynthetic activity, which is then stored in biomass and sediments. According to Lal [5], wetlands store 20–30% of terrestrial carbon at global scale. Among them, coastal wetlands play a key role in sequestering and storing blue carbon from oceans [6]. Nevertheless, degraded ecosystems may rapidly turn from carbon sinks to major sources of greenhouse gases (GHGs), releasing high amounts of CH_4 and CO_2 produced by microbial decomposition of organic matter, e.g., [7]. Methane emissions from wetlands are also augmented by climate change, shifts

in the hydrological regime, eutrophication processes or more in general by processes that support anaerobic conditions in shallow waters, e.g., [3,8,9]. Recently, methane has been receiving increased attention since it is the second-most important GHG in the atmosphere, with a global warming potential 28 times higher than that of CO_2 over a 100-year time frame [10]. Its concentration in air is nearly three times higher than that recorded in 1750, with a stepwise increasing trend characterized by a relatively stable period from 2000 to 2007 and a renewed and rapid growth since 2007 [11–13]. The causes of such impressive CH_4 increment are not fully understood and may include both increasing emissions from anthropogenic sources and/or natural ecosystems and a decline in the oxidative capacity of the atmosphere [14–16]. According to Rosentreter et al. [17], aquatic ecosystems are currently responsible for half of global CH_4 emissions to the atmosphere and their contribution is destined to increase as a consequence of global warming and human alterations. Nevertheless, these estimates are still affected by large uncertainties, mainly because it is not clear how the physico-biogeochemical factors regulate the release of GHGs from aquatic reservoirs to the atmosphere.

Microbial methanogenesis within surface aquatic systems mainly occurs in bottom anoxic sediments, where fresh organic matter accumulates from litterfall, dead plant materials and root exudates, e.g., [18,19], although CH_4 production was also observed under aerobic conditions, e.g., [20–24]. Once released from bottom sediments, CH_4 can upwardly move through the water column and reach the atmosphere via different pathways, including molecular diffusion, ebullition and storage flux, e.g., [25]. The latter occurs under peculiar conditions, being referred to the sudden release of CH_4 either accumulated due to water stratification or trapped by ice formation. Methane ebullition consists in the release of gas bubbles from bottom sediments to the atmosphere with negligible physical, chemical or biological interactions, and, although relevant, it is an intermittent phenomenon. On the other hand, diffusive flux is responsible for the continuous release of a large portion of CH_4 at the water–atmosphere interface and it is the most commonly estimated component of the total flux from surface waters, e.g., [17] and references therein. The diffusive flux is strictly related to the capability of CH_4 released from bottom anoxic sediments to escape oxidation within the water column and, hence, it largely depends on both lake characteristics (e.g., surface area, water depth, mixing regime and trophic state) and external drivers (e.g., temperature, precipitation and landscape), e.g., [25] and references therein [26]. Accordingly, dissolved CH_4 concentrations can be highly variable in both time and space even within a single surface aquatic system, e.g., [27], making estimates of global CH_4 emissions from these ecosystems difficult to be evaluated. Methane emissions from aquatic ecosystems are mainly estimated by direct or indirect measurements of diffusive fluxes from open waters, e.g., [25 and references therein]. Nevertheless, recent studies have highlighted the importance of macrophytes in regulating CH_4 emissions from wetlands, although their influence in promoting or hindering methanogenesis is debated, e.g., [28–32]. In particular, *Phragmites australis* (common reed) was suggested to be particularly effective in transporting gas from the submerged soil to the atmosphere and accreting large amounts of carbon substrates to methanogens enhancing CH_4 production, e.g., [33] and references therein [34,35]. Hence, several knowledge gaps still subsist on how environmental drivers regulate CH_4 emissions from aquatic ecosystems, limiting upscaled efforts to estimate global emissions from surface aquatic systems [36]. Available studies limited to a relatively small number of waterbodies likely produce an underestimation of the global variability in CH_4 emissions, whereas limited data on spatial and temporal variability in CH_4 emissions within single aquatic systems may induce uncertainty on global emissions based on open-water flux values [36] and references therein.

In this paper, we present data on CH_4 diffusive fluxes from two wetlands located in the Versilian Plain (northern Tuscany, Italy), i.e., Porta and Massaciuccoli Lakes. The former is a shallow wetland largely invaded by reeds, which are currently experiencing a progressive decline, and raising annoyances in ambient air quality because of odor problems related to biogenic H_2S emissions from the lake surface [37]. Massaciuccoli Lake has a surface of ca.

700 ha with a wide surrounding marsh interconnected with the sea and is located in a highly anthropized region consisting of both urban and rural areas. Accordingly, these two diverse wetlands, located within the same geographic and climatic zone, offer the opportunity to investigate the physicochemical environmental drivers shaping the spatial and temporal variability of CH_4 diffusive fluxes within each single system. The measurement of both CH_4 and CO_2 diffusive fluxes were complemented with water and dissolved gas chemistry and carbon isotopic composition of dissolved CH_4 and CO_2, contributing to overcoming data scarcity on wetland isotopic signature [38].

2. Materials and Methods

2.1. Study Areas

2.1.1. Porta Lake

Porta Lake (ca. 82 ha) is a wetland located between the coastline (ca. 2.5 km from the sea) and the Apuan Alps. The rocky substratum is made of Tuscan Units formations (*Macigno* sandstones) overlaid by marine to littoral alternations of clay and sand and alluvial deposits [39] and references therein, whereas the dominant soil class in the area is represented by histosols [40]. Lake waters are fed by three springs located at the base of the reliefs on the northeastern margin of the lake (Figure 1a) characterized by widely varying flow rates, ranging from 20.5 to 50 L/s [41]. The spring waters enter the lake through a channel, named Fossa Fiorentina, and slowly flow through excavated channels and ponds until they leave the lake on its southwestern margin, merging the Montignoso creek and, finally, the Versilia River (Figure 1a). A large portion of the wetland is characterized by the presence of wooded areas (dominated by *Salix alba* and *Alnus glutinosa*) and *Phragmites australis* reeds, the latter being affected by reed die-back syndrome (RDBS), e.g., [42–45], since 2016, determining a high accumulation of organic material at the lake bottom, oxygen depletion and emissions of H_2S-rich gases [37].

2.1.2. Massaciuccoli Lake

Massaciuccoli Lake is included in the Migliarino–San Rossore–Massaciuccoli Regional Park, representing an area of international importance under the Ramsar Convention, being recognized as a Site of Importance of the European Community [39], and thus it is regarded as one of the most important wetlands in Italy [46]. It includes (i) a main open-water basin with an average depth of 2 m [39], (ii) a secondary excavated basin (Cava Sisa) in correspondence of a former quarry, with a maximum depth of 24 m [46] and references therein, (iii) an extensive marsh area surrounding the lake northward and eastward and consisting of several pools of different sizes, artificial canals and basins (Figure 1b). The lake waters are fed by precipitation, groundwaters and a series of natural and artificial tributaries, flowing from the mountain belt or fed by water springs (e.g., Case Rosse, Villa Spinola). The surface water network drains agricultural, industrial and urban areas upstream of the lake basin and includes Barra, Fossa Nuova and Quiesa channels (Figure 1b) [47]. The lake has a main emissary, i.e., the Burlamacca canal, that, flowing through the city of Viareggio, directly connects Massaciuccoli Lake to the sea (Figure 1b). The lake waters are affected by severe eutrophication related to water inputs from the drainage of the farmlands and treatment plants of urban wastewater that produce a dramatic reduction of macroalgae and submerged macrophytes and an excessive growth of phytoplankton [46,48,49]. Reed beds are only discontinuously present along the lake and channel shores [50]. Such an environment is thus characterized by variable conditions of water depth, temperature, pH, salinity and redox state (dictated by the availability of free oxygen) along both vertical and lateral profiles, also depending on the contribution of brackish waters due to the marine ingression and fresh, meteoric and runoff waters from the hinterland.

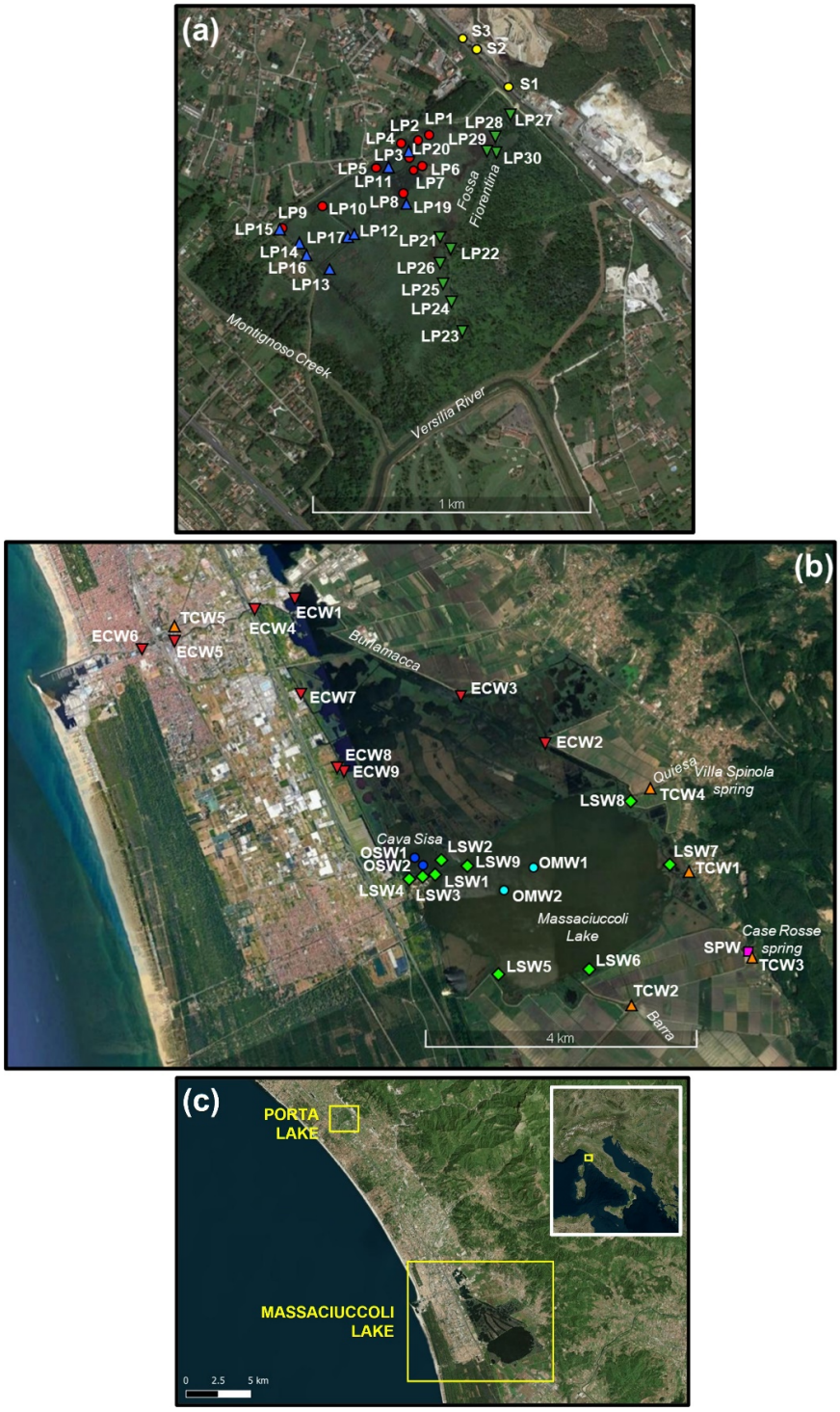

Figure 1. Porta (**a**) and Massaciuccoli (**b**) lakes with the respective sampling sites and their locations (**c**) on the coastal shoreline of western Tuscany (central Italy). In (**a**), circles refer to samples collected in summer, whereas triangles identify those collected in winter. Winter samples are distinguished into waters collected from the boat (blue upward triangles) and those collected from the lakeshores (green downward triangles). The locations of the three springs are indicated by yellow circles. In (**b**), symbols and colors refer to the sample type, as follows: SPW (magenta square), TCW (orange upward triangle), LSW (green diamond), OMW (cyan circles), OSW (blue circles) and ECW (red downward triangle). See text for further explanations. Aerial photographs are from Bing Maps (© 2021 Microsoft, Redmond, WA, USA; www.bing.com/maps, Accessed on 21 October 2021) and Google Earth®.

2.2. Water and Dissolved Gas Sampling

Sampling campaigns were performed in August and December 2020 at Porta Lake and in November 2020 at Massaciuccoli Lake. Sampling activities were carried out between 10:00 and 16:00. Wind speed during sampling campaigns was, on average, around 2.5 m/s (Weather Underground company, San Francisco, CA, USA; https://www.wunderground.com). The coordinates of the sampling sites were recorded using a portable GPS (Garmin® GPSMAP 62, Garmin®, Olathe, KS, USA). Water temperature, pH and Eh values were measured directly in the field through a CRISON MM 40+ multiparameter probe. Sampling procedures within the lakes were performed from a small boat, with the exception of few sampling sites at Porta Lake (from LP21 to LP30), which were collected from the lake shores, mostly in areas of dense vegetation and stagnant water (Figure 1a). Water and dissolved gas sampling were carried out in lakes and canals within 5 cm of the water–air interface. Two aliquots were collected for the analysis of water chemical and isotopic composition as follows: (i) one aliquot of unfiltered water was collected in a 125 mL polyethylene bottle for the analysis of major anions, and (ii) one aliquot of filtered (0.45 µm) and acidified (with 0.5 mL of Suprapur® HCl 30%) water was collected in a 50 mL polyethylene bottle for the analysis of major cations. At Massaciuccoli Lake, two further water aliquots were sampled as follows: (i) in 250 mL polyethylene bottles, containing $SrCl_2$ and NaOH to precipitate the dissolved carbonate species as $SrCO_3$, for isotope analysis of total dissolved inorganic carbon (δ^{13}C-TDIC) [51] and (ii) in 15 mL plastic tubes, after filtration (0.45 µm), for the analysis of stable isotopes of water at selected sites (SPW, TCW2, TCW3, TCW4, TCW5, LSW4, LSW5, LSW7, LSW8, OMW1, OMW2, OSW1, ECW2, ECW3, ECW8 and ECW9). Dissolved gases were sampled by using pre-evacuated glass flasks with a PTFE stopcock. The flask was submerged down to the sampling depth and the stopcock was opened, allowing the water to enter the flask. The dissolved gases partially exsolved in the headspace due to the pressure drop. The flask was filled by 3/4 of its volume with water, before closing the stopcock [52,53]. Within Massaciuccoli Lake system, waters and dissolved gases were further collected along vertical profiles at three selected sites from surface to bottom using the single hose method described in Tassi et al. [54].

2.3. Chemical and Isotopic Analysis of Water and Dissolved Gases

The chemical composition of water was analyzed by (i) acidimetric titration (HCl 0.01 N) for the determination of HCO_3^- and (ii) ion chromatography, using Metrohm 761 and Metrohm 861 chromatographs for the determination of major anions (Cl^-, SO_4^{2-}, NO_3^-, Br^- and F^-) and cations (Na^+, K^+, Ca^{2+} and Mg^{2+}), respectively. The analytical error was <5%. The $^{18}O/^{16}O$ and $D/^1H$ isotopic ratios of water (expressed as $\delta^{18}O$-H_2O and δD-H_2O in‰ vs. V-SMOW) were determined using a Picarro L2130-i analyzer based on cavity ring-down spectroscopy (CRDS). The analysis of the δ^{13}C-TDIC (expressed in‰ vs. V-PDB) was performed by mass spectrometry (MS) using a Finnigan MAT252 instrument on CO_2 recovered after the reaction of $SrCO_3$ with anhydrous phosphoric acid following the procedure described by Salata et al. [55] and a two-step extraction and purification procedure as described in Venturi et al. [56]. The analytical error and the reproducibility for δ^{13}C-TDIC analysis were ±0.05‰ and ±0.1‰, respectively.

The chemical compositions of dissolved gases in the headspace of the sampling flask (CO_2, N_2, Ar + O_2, H_2 and He) were determined using a Shimadzu 15A gas chromatograph equipped with a 5 m long stainless steel column packed with Chromosorb PAW 80/100 mesh and a thermal conductivity detector (TCD), whereas CH_4 was analyzed using a Shimadzu 14A gas chromatograph equipped with a 10 m long stainless steel column packed with Chromosorb PAW 80/100 mesh coated with 23% SP 1700 and a flame ionization detector (FID). Argon and O_2 were analyzed using a Thermo Focus gas chromatograph equipped with a 30 m long capillary molecular sieve column and a TCD. The analytical error for GC analysis was <5% [54] and references therein. The concentrations of dissolved gas species were determined as the sum of the (i) number of moles of each gas in the headspace ($n_{i,g}$), calculated according to the ideal gas law at 20 °C (i.e., laboratory temperature)

considering the partial pressures determined by gas chromatography (P_i), and the volume of the flask headspace (V_{gas}) and (ii) the number of moles of each gas remaining in the liquid ($n_{i,l}$), calculated according to Henry's law, assuming that equilibrium was attained within the flask between the separated gas phase and the liquid, e.g., [54,57–59]. The $^{13}C/^{12}C$ isotopic ratios of CO_2 and CH_4 (expressed as $\delta^{13}C$-CO_2 and $\delta^{13}C$-CH_4, respectively, in ‰ vs. V-PDB) in the headspace of the sampling flask were analyzed by CRDS using a Picarro G2201-i analyzer. The $\delta^{13}C$-CO_2 values were corrected considering the enrichment factor for gas–water isotope equilibrium between gaseous and dissolved CO_2 [56,60].

The chemical and isotopic analyses were carried out respectively by the Laboratory of Fluid Geochemistry and Laboratory of Stable Isotopes (Department of Earth Science, University of Florence), respectively, with the sole exception of the determination of $\delta^{13}C$-TDIC, which was carried out at the Laboratory of Fluids Geochemistry of the INGV, Sezione di Napoli, Osservatorio Vesuviano.

2.4. Diffusive Flux Calculation

The CO_2 and CH_4 diffusive fluxes at the water–air interface (ΦCO_2 and ΦCH_4, respectively) were determined on the basis of the measured dissolved gas concentrations ($C_{i,w}$, in mol/L), according to the thin boundary layer (TBL) model [61] as follows:

$$\Phi_i = \beta k_i \left(C_{i,w} - C_{i,eq}\right) \tag{1}$$

where $C_{i,eq}$ is the dissolved gas concentration calculated assuming equilibrium with the atmosphere (based on gas solubilities as a function of temperature and salinity [62]), β is the chemical enhancement applicable for CO_2 only (see below) and k_i is the gas transfer velocity (in cm h^{-1}). The k_i values were estimated as follows:

$$k_i = k_{600,i} \left(\frac{Sc_i}{600}\right)^x \tag{2}$$

where (i) $k_{600,i}$ is the k_i value for each gas normalized to 600, (ii) x is dependent upon the roughness of the water surface (−0.67 or −0.5 for wind speed <3 m s^{-1} or >3 m s^{-1}, respectively [63]) and (iii) Sc_i is the Schmidt number. The Sc_i values were calculated for each gas based on temperature, according to the fourth order polynomial fits proposed by Wanninkhof [62]. The $k_{600,i}$ values were calculated from local wind speed using the following empirical relationships [63,64]:

$$k_{600,i} = 0.23{U_{10}}^2 + 0.1U_{10} \tag{3}$$

$$k_{600,i} = 0.72U_{10} \tag{4}$$

where U_{10} is the wind speed at a height of 10 m. The latter was calculated from average wind speed recorded during the sampling campaigns (Weather Underground company, San Francisco, CA, USA; https://www.wunderground.com) as described in Crusius and Wanninkhof [63] and references therein.

The chemical enhancement factor β for the determination of ΦCO_2 values was computed according to Hoover and Berkshire [65] and Wanninkhof and Knox [66] as follows:

$$\beta = \frac{\tau}{(\tau - 1) + \frac{tanh\left[\left(r\tau D^{-1}\right)^{0.5} Dk_{CO_2}^{-1}\right]}{\left[\left(r\tau D^{-1}\right)^{0.5} Dk_{CO_2}^{-1}\right]}} \tag{5}$$

where: (i) D is the molecular diffusivity (in cm^2/s), calculated as $D = 14.6836 \times 10^{-5} \times \left[\frac{(273.15+t(^\circ C))}{217.2056} - 1\right]^{1.997}$ [67] ; (ii) r (in s^{-1}) is the combined rate constant for the hydration of CO_2, calculated as $r = r_1 + r_2 K_w^* a_H^{-1}$, where r_1 (in s^{-1}) and r_2 (in $Lmol^{-1}s^{-1}$) are the CO_2 hydration rate and the CO_2 hydroxylation rate constants, respectively [68], K_w* is the

equilibrium constant for water and a_H is the activity coefficient for the hydrogen ion; (iii) $\tau = 1 + \frac{a_H^2}{(K'_1 K'_2 + K'_1 a_H)}$, where K'_1 and K'_2 are the first and second equilibrium constants for carbonic acid, respectively [69].

The overall diffusive flux in terms of CO_2 equivalents (ΦCO_{2eq}) was calculated as:

$$\Phi CO_{2eq} = \Phi CO_{2eq} + GWP_{CH4} \times \Phi CH_4 \quad (6)$$

where GWP_{CH4} is the global warming potential value of CH_4 over a 100-year time horizon (i.e., 28 [10]).

3. Results

3.1. The Chemical Features of Porta Lake

Porta Lake waters were characterized by comparable pH values in summer and winter, i.e., ranging from 7.18 to 8.11 and from 7.17 to 7.78, respectively (Table 1), whereas TDS (total dissolved solids) values were from 733 to 787 mg/L in summer and from 618 to 839 mg/L in winter (Table 1). The Eh values ranged from −295 to 96 mV, with the lowest values recorded in August (Table 1). Water temperatures were from 23.7 to 31.2 °C in summer and from 7.7 to 16.1 °C in winter. In the sampling sites, the lake depth varied from 20 to 70 cm in summer and from 5 to 150 cm in winter, with an increase in the water column depth of more than 40 cm in December with respect to that of August (LP10, LP18; Table 1). The chemical composition of Porta Lake waters was dominated by the Ca^{2+}-SO_4^{2-} facies, in agreement with the composition of spring waters feeding the lake (S1, S2 and S3), with the sole exception of few samples collected in winter (i.e., LP21, LP22, LP23, LP24, LP25 and LP26) and located in the easternmost margin of the lake (Figure 1a) which displayed a Ca^{2+}-HCO_3^- geochemical facies. The lake waters were enriched in NH_4^+ and generally depleted in NO_3 with respect to the spring waters (Table 1). Fluoride and Br^- concentrations were relatively low (≤0.76 and ≤0.2 mg/L, respectively).

Dissolved gases were dominated by N_2, generally followed by either CH_4 or O_2, whereas CO_2 was, in most samples, the third most abundant compound (Table 2). Dissolved oxygen concentrations were higher in winter (from 0.011 to 0.16 mmol/L) than in summer (from 0.005 to 0.11 mmol/L). On the contrary, CH_4 showed, on average, higher concentrations in summer (mean: 0.26 mmol/L) than in winter (mean: 0.20 mmol/L). The measured N_2/Ar ratios were consistent with those of air-saturated water (ASW), i.e., around 40. The $\delta^{13}C$-CH_4 values ranged from −57.3 to −40.8‰ vs. V-PDB, whereas those of CO_2 values varied from −26.7 to −17.6‰ vs. V-PDB (Table 2).

Table 1. Water column depth (w.c.d., in cm), temperature (in °C), pH, redox potential (Eh, in mV) and chemical composition of the main solutes in water samples (in mg/L) from Porta Lake. TDS (total dissolved solids, in mg/L) values are also reported.

	ID	E	N	w.c.d.	T	pH	Eh	HCO_3	Cl	SO_4	Na	K	Ca	Mg	NH_4	NO_3	F	Br	TDS
summertime	LP1	593,756	4,872,054	40	23.7	7.41	>−153	215	27	328	16	1.7	163	32	0.33	2.1	0.76	0.09	787
	LP2	593,716	4,872,032	20	25.6	7.18	−295	204	24	301	16	2.0	153	32	0.23	0.11	0.33	0.08	733
	LP3	593,687	4,871,974	70	26.7	7.4	89	201	26	328	16	1.7	161	32	0.08	0.61	0.44	0.09	768
	LP4	593,661	4,872,021	50	28.7	7.47	−32	192	26	325	17	2.5	160	33	0.11	0.06	0.49	0.08	755
	LP5	593,573	4,871,929	40	27.1	7.4	−66	205	26	323	17	2.2	162	32	0.16	0.40	0.33	0.09	768
	LP6	593,732	4,871,939	30	31.2	8.11	−129	192	27	327	17	1.9	160	32	0.27	0.25	0.47	0.09	757
	LP7	593,704	4,871,926	20	30.1	7.54	−192	205	26	320	17	1.4	161	32	0.38	0.04	0.32	0.08	763
	LP8	593,666	4,871,844	70	28.1	7.64	20	199	27	328	17	2.2	163	33	0.09	0.45	0.36	0.09	769
	LP9	593,226	4,871,708	40	27.7	7.3	−51	201	27	307	17	1.6	160	32	0.20	0.14	0.61	0.09	746
	LP10	593,377	4,871,788	30	28.5	7.4	−120	201	27	334	16	2.1	160	32	0.21	0.13	0.38	0.09	773
wintertime	LP11	593,613	4,871,927	115	11.3	7.4	96	217.16	20	281	19	1.3	150	30	0.09	1.97	0.24	0.06	722
	LP12	593,493	4,871,693	40	10.3	7.5	35	216	20	272	19	2.3	147	30	0.08	1.46	0.23	0.15	708
	LP13	593,402	4,871,555	70	9.4	7.4	87	203.74	18	273	18	2.1	130	27	0.08	0.37	0.18	0.09	672
	LP14	593,298	4,871,649	40	10.0	7.55	24	220	19	245	17	2.4	138	26	0.11	1.47	0.22	0.08	670
	LP15	593,219	4,871,708	110	10.2	7.48	95	220.82	22	285	20	3.6	151	30	0.11	1.86	0.36	0.09	735
	LP16	593,325	4,871,615	20	9.6	7.49	12	219	19	215	18	2.7	118	24	0.37	0.82	0.80	0.09	618
	LP17	593,473	4,871,679	40	10.5	7.45	19	219.6	19	258	19	1.2	137	30	0.28	1.42	0.24	0.06	686
	LP18	593,376	4,871,786	70	10.6	7.54	52	218.38	19	274	21	4.3	143	31	0.13	1.60	0.21	0.08	713
	LP19	593,680	4,871,797	70	10.8	7.53	4	214.72	21	261	20	2.6	136	30	0.53	1.93	0.20	0.08	688
	LP20	593,684	4,871,988	150	11.6	7.5	81	214.72	19	257	19	1.6	135	30	0.19	2.68	0.28	0.08	680
	LP21	593,805	4,871,686	10	9.5	7.2	−77	330.62	46	129	25	33	105	33	0.51	1.02	0.13	0.17	703
	LP22	593,837	4,871,648	10	7.7	7.25	−80	386	36	39	22	7.9	95	31	0.79	0.48	0.18	0.12	618
	LP23	593,885	4,871,350	10	8.2	7.52	12	397.72	70	30	44	7.1	95	34	0.27	0.04	0.08	0.22	678
	LP24	593,841	4,871,464	40	9.4	7.5	−54	431.88	33	61	32	5.7	116	34	0.73	0.02	0.17	0.14	715
	LP25	593,814	4,871,521	20	9.8	7.6	−31	322.08	26	145	25	4.4	122	31	0.54	0.02	0.19	0.12	676
	LP26	593,800	4,871,601	5	11.2	7.6	−98	272.06	23	188	20	3.8	128	30	0.61	3.26	0.26	0.11	669
	LP27	594,047	4,872,130	30	16.1	7.17	85	212.28	24	363	18	2.7	177	34	0.05	7.68	0.43	0.09	839
	LP28	593,996	4,872,049	20	10.8	7.71	−140	262.3	25	217	22	4.9	124	29	0.43	0.70	0.45	0.04	686
	LP29	593,972	4,872,003	10	12.0	7.78	27	220.82	19	323	21	3.0	157	34	0.04	5.08	0.21	0.08	784
	LP30	593,997	4,871,997	60	16.1	7.69	53	217.16	26	337	24	3.0	169	33	0.04	7.20	0.32	0.05	816
spring waters	S1	594,043	4,872,228		17.0	7.8	155	212	32	286	23	2.3	156	29	0.02	7.2	0.45	0.09	748
	S2	593,923	4,872,362		17.5	7.92	141	195	20	375	12	2.2	171	33	0.02	7.0	0.39	0.05	814
	S3	593,876	4,872,404		18.0	7.76	160	195	19	356	12	2.5	171	33	0.02	6.7	0.42	0.04	795

Table 2. Chemical composition (in mmol/L) of the main dissolved gases from Porta Lake. The isotopic composition of carbon in CO_2 and CH_4 ($\delta^{13}C$-CO_2 and $\delta^{13}C$-CH_4, respectively, in ‰ vs. V-PDB) is also reported, as well as the CO_2, CH_4 and CO_{2eq} diffusive fluxes (ΦCO_2, ΦCH_4 and ΦCO_{2eq}, respectively, in g m^{-2} d^{-1}).

ID	CO_2	N_2	Ar	CH_4	O_2	$\delta^{13}C$-CO_2	$\delta^{13}C$-CH_4	ΦCH_4	ΦCO_2	ΦCO_{2eq}
LP1	0.09	0.53	0.013	0.25	0.011	−21.5	−53.3	2.25	16.6	79.6
LP2	0.14	0.51	0.013	0.26	0.005	−20.9	−53.4	2.49	20.6	90.4
LP3	0.11	0.52	0.013	0.17	0.084	−18.7	−50.5	1.69	24.1	71.3
LP4	0.09	0.53	0.014	0.29	0.012	−20.8	−54.7	3.06	23.8	110
LP5	0.08	0.49	0.012	0.31	0.011	−21.3	−54.9	3.11	17.0	104
LP6	0.07	0.51	0.013	0.33	0.012	−21.8	−55.6	3.77	52.8	158
LP7	0.13	0.49	0.013	0.45	0.005	−22.1	−57.3	4.97	43.5	183
LP8	0.13	0.52	0.013	0.12	0.11	−17.6	−45.2	1.24	46.4	81.2
LP9	0.09	0.55	0.014	0.21	0.055	−21.3	−52.8	2.15	17.0	77.2
LP10	0.09	0.52	0.013	0.24	0.017	−21.4	−51.7	2.52	20.9	91.5
LP11	0.11	0.68	0.017	0.08	0.15	−18.4	−41.1	0.472	9.73	23.0
LP12	0.08	0.71	0.018	0.15	0.078	−18.5	−46.9	0.853	6.94	30.8
LP13	0.12	0.69	0.018	0.09	0.13	−18.7	−43.6	0.495	9.50	23.3
LP14	0.09	0.67	0.017	0.11	0.11	−18.7	−42.5	0.619	8.57	25.9
LP15	0.08	0.69	0.017	0.07	0.16	−18.2	−41.7	0.397	6.68	17.8
LP16	0.05	0.72	0.018	0.12	0.061	−18.6	−40.8	0.665	3.13	21.7
LP17	0.07	0.69	0.017	0.11	0.088	−18.4	−43.5	0.630	5.44	23.1
LP18	0.09	0.68	0.017	0.09	0.14	−18.4	−42.7	0.518	8.82	23.3
LP19	0.11	0.67	0.017	0.21	0.053	−19.7	−50.9	1.22	11.4	45.5
LP20	0.08	0.69	0.018	0.07	0.15	−19.8	−41.2	0.418	7.69	19.4
LP21	0.13	0.65	0.016	0.38	0.023	−23.3	−54.8	2.10	7.83	66.5
LP22	0.14	0.66	0.016	0.41	0.011	−24.2	−55.6	2.11	8.20	67.3
LP23	0.15	0.65	0.017	0.17	0.081	−26.7	−44.6	0.892	13.7	38.7
LP24	0.14	0.65	0.016	0.35	0.016	−23.9	−55.6	1.92	13.3	67.2
LP25	0.12	0.66	0.017	0.34	0.018	−21.9	−54.2	1.90	13.1	66.3
LP26	0.16	0.66	0.017	0.45	0.013	−21.1	−56.7	2.65	20.4	94.6
LP27	0.09	0.65	0.016	0.11	0.16	−18.0	−50.0	0.772	7.18	28.8
LP28	0.11	0.66	0.016	0.43	0.011	−21.9	−57.3	2.49	14.7	84.5
LP29	0.08	0.65	0.016	0.09	0.11	−18.3	−47.4	0.545	11.6	26.9
LP30	0.07	0.65	0.016	0.11	0.14	−18.9	−47.1	0.772	11.7	33.3

3.2. CH_4 and CO_2 Diffusive Fluxes at Porta Lake

The CH_4 and CO_2 diffusive fluxes at the water–air interface calculated according to the TBL model are reported in Table 2. The ΦCH_4 values varied from 1.24 (LP8) to 4.97 (LP7) g CH_4 m^{-2} day^{-1} in summer, whereas lower values were measured in winter, ranging from 0.397 (LP15) to 2.65 (LP26) g CH_4 m^{-2} day^{-1}. Similarly, the calculated ΦCO_2 values were positive, with higher values in summer (from 16.6 to 52.8 g CO_2 m^{-2} day^{-1}) with respect to winter (from 3.13 to 20.4 g CO_2 m^{-2} day^{-1}). In terms of CO_2 equivalents, diffusive fluxes from Porta Lake varied from 71 (LP3) to 183 (LP7) g CO_{2eq} m^{-2} in summer and from 18 (LP15) to 95 (LP26) g CO_{2eq} m^{-2} in winter.

3.3. The Chemical Features of Massaciuccoli Lake System

The waters collected from Massaciuccoli Lake system referred to a wide variety of environments, i.e., open waters from both (i) the main Massaciuccoli Lake basin (OMW) and (ii) the excavated Cava Sisa basin (OSW), (iii) waters collected close to the lake shores (LSW), (iv) Case Rosse spring water (SPW), which is one of the springs feeding the lake [47], (v) several tributary channels discharging waters in Massaciuccoli Lake or in the Burlamacca canal (TCW) and (vi) emissary channels (ECW), including the Burlamacca canal (Figure 1b).

The collected surface waters were characterized by pH values ranging from 7.8 to 8.5 and T from 13.7 to 17.4 °C (Table 3). The SPW sample was characterized by a Ca^{2+}-HCO_3^- composition and TDS and Eh values of 439 mg/L and 645 mV, respectively. Nitrate was present at a relatively high concentration, i.e., 6.1 mg/L (Table 3). The isotopic composition of this spring was characterized by $\delta^{18}O$-H_2O and δD-H_2O values of −6.07 and −35.1 in‰ vs. V-SMOW, respectively, whereas the $\delta^{13}C$-TDIC value was −14.8‰ vs. V-PDB (Table 3). Conversely, the TCW samples showed TDS values ranging from 636 (TCW4) to 2360 (TCW2) mg/L and Eh values varying from 117 (TCW1) to 223 (TCW2) mV. They were characterized by a Na^+-Cl^- composition, with the sole exception of TCW4 that showed Ca^{2+} and SO_4^{2-} as dominant cationic and anionic species (Table 3). The water column depth varied from 0.5 to 2 m. On average, the TCW samples were characterized by the highest NH_4^+ and NO_3^- concentrations, up to 1.7 and 31 mg/L, respectively, in TCW5 (Table 3). The $\delta^{18}O$-H_2O and δD-H_2O values were ranging from −6.33 (TCW4) to −1.68 (TCW3)‰ vs. V-SMOW and from −36.7 (TCW4) to −13.3 (TCW3)‰ vs. V-SMOW, respectively (Table 3). The $\delta^{13}C$-TDIC values ranged from −13.8 (TCW4 and TCW5) to −12.9 (TCW3)‰ vs. V-PDB (Table 3).

On average, the ECW samples displayed higher TDS values, which ranged from 1782 (ECW8) to 3821 (ECW1) mg/L, and comparable Eh, varying from 133 (ECW1) to 219 (ECW9) mV, whilst the water column depth ranged from 0.7 to 1 m. The chemical composition of the ECW samples was Na^+-Cl^-, with significantly higher concentrations of Na^+, Cl^-, K^+ and Br^- with respect to the TCW samples (Table 3). The NH_4^+ and NO_3^- concentrations were up to 0.38 and 17 mg/L, respectively (ECW8). The isotopic composition of water in the ECW samples showed a relative enrichment in the heavier isotopes with respect to those of TCW, with $\delta^{18}O$-H_2O and δD-H_2O values varying from −3.87 (ECW8) to −1.28 (ECW3)‰ vs. V-SMOW and from −24.1 (ECW8) to −11.6 (ECW3 and ECW9)‰ vs. V-SMOW, respectively (Table 3). The $\delta^{13}C$-TDIC values ranged from −14.5 (ECW8) to −12.2 (ECW7)‰ vs. V-PDB (Table 3).

Table 3. Water column depth (w.c.d., in m), temperature (in °C), pH, redox potential (Eh, in mV) and chemical composition of the main solutes in water samples (in mg/L) from Massaciuccoli Lake. TDS (total dissolved solids, in mg/L) values are also reported, along with the isotopic composition of carbon in total dissolved inorganic carbon (δ^{13}C-TDIC, in ‰ vs. V-PDB) and of oxygen and hydrogen in water (δ^{18}O-H_2O and δD-H_2O, in ‰ vs. V-SMOW).

	ID	E	N	w.c.d.	T	pH	Eh	HCO_3	Cl	SO_4	Na	K	Ca	Mg	NH_4	NO_3	F	Br	TDS	δ18O-H_2O	δD-H_2O	δ13C-TDIC
spring water	SPW	609,910	4,853,354	0	15.4	7.8	645	263	40	13	24	2	85	6.2	0.04	6.1	0.3	0.1	439	−6.07	−35.1	−14.75
tributary channels	TCW1	609,028	4,854,555	2	17.2	8.4	117	206	525	395	361	15	141	61	0.13	0.39	0.5	1.7	1706.7			−13.6
	TCW2	608,185	4,852,544	1	14.3	7.9	223	451	726	450	396	9	222	91	0.81	11	0.5	3.3	2360.1	−3.86	−23.8	−13.03
	TCW3	609,931	4,853,285	1	14.1	7.9	221	222	811	222	423	20	110	68	0.16	0.2	0.4	3	1879.8	−1.68	−13.3	−12.9
	TCW4	608,460	4,855,717	0.5	16.5	8.1	209	166	20	281	10	0	141	11	0.05	6.3	0.4	0.1	636	−6.33	−36.7	−13.79
	TCW5	601,245	4,858,083	1.5	16.3	8.2	201	274	246	178	141	11	115	26	1.72	31	0.5	0.7	1025	−5.61	−33.6	−13.75
lake shores	LSW1	605,253	4,854,472	3	16.1	8.1	209	212	981	449	622	26	132	99	0.32	0.21	0.3	2.5	2524.4			−11.7
	LSW2	605,329	4,854,662	3	15.9	8.2	179	185	998	433	611	26	128	97	0.25	0.26	0.6	2.6	2481.7			−12.6
	LSW3	605,053	4,854,417	3	17.1	8.3	127	209	1040	431	627	26	140	100	0.2	0.21	0.4	2.4	2576.2			−12.9
	LSW4	604,864	4,854,403	1.8	17	8.5	135	198	984	452	614	25	131	98	0.23	0.23	0.5	2.4	2505.3	−0.99	−10.1	−13.5
	LSW5	606,212	4,852,985	0.8	14.5	7.9	164	224	993	366	610	31	138	95	0.24	1.3	0.6	2.9	2462.1	−1.22	−10.7	−12.4
	LSW6	607,547	4,853,088	0.8	14.5	7.9	223	240	989	399	591	27	136	94	0.23	0.13	0.4	4.1	2480.8			−12.84
	LSW7	608,772	4,854,627	1	16.1	8	−179	231	1078	297	618	32	138	98	0.3	0	0.5	4.3	2497.1	−1.37	−11.1	−13.06
	LSW8	608,132	4,855,571	1	15.4	7.8	184	281	1125	267	593	27	152	96	0.48	0.24	0.7	3.9	2546.3	−1.8	−14.4	−13.82
	LSW9	605,717	4,854,577	2.5	14.8	8.2	195	209	1039	246	612	26	130	96	0.14	0.15	0.4	3.8	2362.5			−14.23
emissary channels	ECW1	603,052	4,858,611	1	17.4	8.4	133	211	1730	495	1020	42	172	147	0.13	0.28	0.4	3.6	3821.5			−14.1
	ECW2	606,877	4,856,416	0.7	16	7.9	210	219	1166	302	611	28	135	92	0.11	0.38	0.7	4	2558.2	−2.4	−16.8	−13.13
	ECW3	605,588	4,857,131	0.7	16.8	8.1	211	219	1515	304	763	47	150	118	0.18	0.36	0.5	5	3122.1	−1.28	−11.6	−12.55
	ECW4	602,446	4,858,415	1	16.5	8.3	202	219	1672	306	829	34	151	120	0.11	0.22	0.6	6.4	3338.3			−12.7
	ECW5	601,273	4,857,944	1	16.2	8.4	208	227	1555	350	810	29	152	122	0.14	0.39	0.4	6.5	3252.4			−13.18
	ECW6	600,820	4,857,784	1	16.1	8.2	196	231	1490	297	753	32	146	113	0.13	0.75	0.7	5.2	3068.8			−12.25
	ECW7	603,180	4,857,119	0.7	16.3	8.4	193	241	1368	273	735	33	139	111	0.18	0.01	0.6	5.2	2906			−12.17
	ECW8	603,748	4,856,001	0.7	15.7	8.2	201	323	727	121	389	22	116	64	0.38	17	0.5	2.6	1782.5	−3.87	−24.1	−14.51
	ECW9	603,842	4,855,965	0.7	16.7	8.1	219	244	1274	263	664	29	138	103	0.15	0.42	0.5	5.5	2721.5	−1.38	−11.6	−12.98
main basin (Massaciuccoli lake)	OMW1 (0 m)	606,696	4,854,546	3	14.1	7.8	214	220	996	320	590	28	129	90	0.22	0.02	0.4	4.1	2377.7	−1.22	−11.2	−13.78
	OMW1 (1 m)	606,696	4,854,546		13.9	7.7	214	212	1245	331	634	23	143	99	0.23	0.04	0.3	4.2	2691.8			−16.79
	OMW1 (2 m)	606,696	4,854,546		13.5	7.6	236	208	1196	255	639	22	138	101	0.23	0.01	0.4	5.1	2564.7			−16.68
	OMW1 (3 m)	606,696	4,854,546		13.5	7.4	230	213	1312	307	639	27	140	100	0.25	0.13	0.4	5.4	2744.2			−16.71
main basin (Massaciuccoli lake)	OMW2 (0 m)	606,275	4,854,208	2.5	13.7	8.3	193	214	1261	296	629	28	138	99	0.2	0.01	0.5	4.8	2670.5	−1.1	−10.8	−13.91
	OMW2 (1 m)	606,275	4,854,208		13.7	8.3	183	213	1225	285	632	25	143	99	0.2	0.04	0.6	4.3	2627.1			−13.34
	OMW2 (2 m)	606,275	4,854,208		13.9	7.9	180	214	1213	289	638	24	139	100	0.23	0.12	0.5	4.1	2622			−13.51
	OMW2 (2.5 m)	606,275	4,854,208		13.9	7.9	190	212	1209	284	626	23	138	98	0.13	0.22	0.5	3.9	2594.7			−13.55

Table 3. *Cont.*

	ID	E	N	w.c.d.	T	pH	Eh	HCO_3	Cl	SO_4	Na	K	Ca	Mg	NH_4	NO_3	F	Br	TDS	δ18O-H_2O	δD-H_2O	δ13C-TDIC
Cava Sisa	OSW1 (0 m)	604,945	4,854,675	16	15.1	8.2	188	213	1042	313	616	27	128	96	0.15	0.24	0.5	4.4	2440.2	−1.17	−10.7	−13.49
	OSW1 (1 m)	604,945	4,854,675		14.8	8.1	164	212	1206	275	608	19	129	95	0.11	0.07	0.4	4.3	2548.9			−13.25
	OSW1 (2 m)	604,945	4,854,675		14.8	8.1	149	212	1171	267	611	24	130	95	0.16	0.2	0.3	4.2	2514.9			−13.86
	OSW1 (4 m)	604,945	4,854,675		14.7	8.1	138	211	1176	268	614	25	130	96	0.11	0.2	0.4	3.8	2524.5			−14.87
	OSW1 (6 m)	604,945	4,854,675		14.7	8.1	137	217	1247	318	624	30	133	96	0.11	0.35	0.5	4.1	2670			−14.59
	OSW1 (8 m)	604,945	4,854,675		14.7	8.1	146	207	1169	266	622	21	131	97	0.14	0.15	0.5	3.8	2517.6			−14.3
	OSW1 (10 m)	604,945	4,854,675		14.5	8.2	−11	212	1252	288	601	24	128	95	0.14	0.2	0.5	3.9	2604.7			−16.33
	OSW1 (12 m)	604,945	4,854,675		10.9	7.5	−202	272	1160	268	621	91	138	94	1.5	0.1	0.5	3.6	2649.7			−16.68
	OSW1 (14 m)	604,945	4,854,675		10	7.4	−212	297	1170	267	577	29	143	92	2.03	0.08	0.6	3.7	2581.4			−16.7
	OSW1 (16 m)	604,945	4,854,675		9.9	7.2	−215	314	1101	268	574	22	138	92	2.7	0.36	0.7	3.4	2516.1			−17.01
	OSW2	605,069	4,854,569	15	16.5	8.2	163	209	1050	444	640	29	135	100	0.18	0.18	0.4	2.6	2610.4			−13.1

The surface waters from Massaciuccoli Lake (OMW) and Cava Sisa (OSW) were characterized by comparable TDS and Eh values, ranging from 2378 (OMW1) to 2670 (OMW2) mg/L and from 163 (OSW2) to 214 (OMW1) mV, respectively, and displayed a Na^+-Cl^- geochemical facies (Table 3). The $\delta^{18}O$-H_2O and δD-H_2O values of surface waters were comparable between the two basins, ranging from −1.22 (OMW1) to −1.10 (OMW2)‰ vs. V-SMOW and from −11.2 (OMW1) to −10.7 (OSW1)‰ vs. V-SMOW, respectively (Table 3). Similarly, the carbon isotopic composition of TDIC was around −13.8‰ vs. V-PDB in OMW samples and −13.3‰ vs. V-PDB in the OSW samples (Table 3).

The water column depth significantly differed, varying from 2.5 to 3 m (OMW) and from 15 to 16 m (OSW). Different from the OMW sampling sites, a clear stratification was observed at OSW, with a sharp decrease in Eh, pH and T values between 8 and 12 m depth (Table 3). The bottom waters along the OSW profile were characterized by reduced conditions and higher NH_4^+ concentrations (up to 2.7 mg/L) with respect to those measured in the shallower waters (≤0.14 mg/L). These concentrations were two orders of magnitude higher than those determined at the bottom of Massaciuccoli Lake main basin, i.e., 0.25 and 0.13 mg/L at OMW1 and OMW2, respectively (Table 3). The carbon isotopic composition of TDIC showed different trends along the vertical profile in the sampled sites. In Massaciuccoli Lake, OMW1 and OMW2 showed rather constant $\delta^{13}C$-TDIC values with depth, i.e., around −16.7 and −13.6‰ vs. V-PDB, respectively, with the sole exception of the OMW1 surface water that was enriched in the heavier isotope with respect to deeper waters (Table 3). At Cava Sisa, the $\delta^{13}C$-TDIC values showed a clear shift between 8 and 10 m depth, ranging from −14.9 to −13.3‰ vs. V-PDB in shallow waters and from −17.0 to −16.3‰ vs. V-PDB in deep waters (Table 3).

The LSW samples were characterized by TDS values ranging from 2363 (LSW9) to 2576 (LSW3) mg/L. Overall, the Eh values ranged from 127 (LSW3) to 223 (LSW6) mV, with the sole exception of the LSW7 sample, which displayed an Eh value of −179 mV; the water column depth varied from 0.8 to 3 m (Table 3). The chemical composition was dominated by Na^+ and Cl^-, with higher concentrations of NH_4^+ and NO_3^- with respect to those recorded in the OMW and OSW surface water samples, i.e., up to 0.48 (LSW8) and 1.3 (LSW5) mg/L, respectively (Table 3). The isotopic composition of water was comparable with that of samples from open waters, the $\delta^{18}O$-H_2O and δD-H_2O values being from −1.80 (LSW8) to −0.99 (LSW4)‰ vs. V-SMOW and from −14.4 (LSW8) to −10.1 (LSW4)‰ vs. V-SMOW, respectively (Table 3). The $\delta^{13}C$-TDIC values ranged from −14.2 (LSW9) to −11.7 (LSW1)‰ vs. V-PDB (Table 3).

The chemical composition of dissolved gases was dominated by N_2 in all of the collected surface waters, with concentrations ranging from 0.54 (LSW4 and TCW3) to 0.66 (LSW8) mmol/L (Table 4). The measured N_2/Ar ratios were varying around that of ASW, i.e., from 38 to 43. The second most abundant gas was O_2, with concentrations ranging from 0.056 (LSW7) to 0.31 (TCW4) mmol/L, with the sole exception of the LSW7 sample that was characterized by CH_4 as the second most abundant gas after N_2. Overall, the dissolved CH_4 concentrations varied from 0.003 (OMW2) to 0.23 (LSW7) mmol/L, with values averagely higher in the LSW, TCW and ECW samples with respect to those measured in the SPW, OMW and OSW samples (Table 4). The dissolved CO_2 concentrations ranged from 0.006 (SPW) to 0.15 (LSW7) mmol/L (Table 4). The carbon isotopic composition of CO_2 and CH_4 showed a general increase in CO_2 and CH_4 concentrations, with $\delta^{13}C$-CO_2 and $\delta^{13}C$-CH_4 values ranging from −22.0 (LSW4) to −9.20 (LSW3)‰ vs. V-PDB and from −60.4 (LSW7) to −33.6 (SPW)‰ vs. V-PDB, respectively (Table 4).

Table 4. Chemical composition (in mmol/L) of the main dissolved gases from Massaciuccoli Lake. The isotopic composition of carbon in CO_2 and CH_4 ($\delta^{13}C$-CO_2 and $\delta^{13}C$-CH_4, respectively, in ‰ vs. V-PDB) is also reported, as well as the CO_2, CH_4 and CO_{2eq} diffusive fluxes (ΦCO_2, ΦCH_4 and ΦCO_{2eq}, respectively, in g m^{-2} d^{-1}).

ID	CO_2	N_2	Ar	CH_4	O_2	$\delta^{13}C$-CO_2	$\delta^{13}C$-CH_4	ΦCH_4	ΦCO_2	ΦCO_{2eq}
SPW	0.01	0.59	0.014	0.005	0.25	−13.0	−33.6	0.034	−3.03	−2.07
TCW1	0.06	0.62	0.015	0.012	0.16	−15.6	−44.5	0.087	25.7	28.2
TCW2	0.02	0.55	0.013	0.0076	0.19	−17.1	−35.9	0.050	0.500	1.90
TCW3	0.03	0.54	0.013	0.014	0.18	−18.5	−45.6	0.092	3.78	6.35
TCW4	0.01	0.65	0.016	0.0058	0.31	−13.5	−36.1	0.041	−3.49	−2.33
TCW5	0.04	0.65	0.016	0.017	0.18	−15.4	−43.6	0.120	7.39	10.7
LSW1	0.04	0.58	0.014	0.011	0.19	−13.4	−40.4	0.077	6.82	8.98
LSW2	0.04	0.55	0.014	0.015	0.16	−15.9	−36.1	0.104	10.5	13.5
LSW3	0.06	0.63	0.015	0.021	0.15	−9.2	−48.7	0.152	20.6	24.8
LSW4	0.09	0.54	0.014	0.016	0.12	−22.0	−49.4	0.116	39.9	43.1
LSW5	0.09	0.63	0.016	0.026	0.15	−16.0	−49.3	0.172	17.2	22.1
LSW6	0.08	0.57	0.015	0.025	0.17	−17.5	−50.1	0.166	15.7	20.3
LSW7	0.15	0.63	0.016	0.23	0.056	−18.9	−60.4	1.61	43.9	89.0
LSW8	0.06	0.66	0.016	0.019	0.12	−15.4	−48.8	0.130	11.3	15.0
LSW9	0.05	0.63	0.016	0.0065	0.15	−15.3	−40.8	0.044	3.89	5.11
ECW1	0.10	0.56	0.013	0.016	0.13	−18.8	−47.6	0.117	41.8	45.1
ECW2	0.07	0.64	0.015	0.012	0.15	−17.4	−45.5	0.084	15.8	18.1
ECW3	0.06	0.61	0.015	0.016	0.17	−16.5	−45.1	0.115	15.3	18.5
ECW4	0.03	0.56	0.014	0.0085	0.16	−13.4	−37.3	0.060	6.79	8.48
ECW5	0.03	0.57	0.015	0.011	0.19	−14.8	−42.3	0.077	5.09	7.26
ECW6	0.03	0.63	0.015	0.015	0.15	−16.6	−43.4	0.105	3.01	5.96
ECW7	0.09	0.64	0.016	0.011	0.15	−14.7	−41.9	0.078	35.5	37.7
ECW8	0.01	0.61	0.015	0.016	0.18	−13.2	−44.8	0.111	−2.84	0.261
ECW9	0.07	0.61	0.016	0.012	0.19	−17.0	−46.6	0.086	20.0	22.4
OMW1 (0 m)	0.02	0.55	0.014	0.0035	0.19	−13.4	−44.5	0.023	−0.03	0.613
OMW1 (1 m)	0.04	0.58	0.014	0.0056	0.18	−12.7	−44.6			
OMW1 (2 m)	0.05	0.64	0.016	0.0071	0.15	−13.0	−44.2			
OMW1 (3 m)	0.08	0.63	0.016	0.0088	0.13	−13.6	−47.8			
OMW2 (0 m)	0.02	0.57	0.014	0.0031	0.18	−12.7	−43.3	0.020	1.09	1.65
OMW2 (1 m)	0.04	0.59	0.015	0.0049	0.18	−13.7	−43.5			
OMW2 (2 m)	0.06	0.54	0.014	0.0063	0.15	−13.9	−45.6			
OMW2 (2.5 m)	0.10	0.56	0.014	0.0078	0.14	−14.2	−47.9			
OSW1 (0 m)	0.07	0.62	0.016	0.0087	0.15	−14.6	−43.7	0.059	5.95	7.60
OSW1 (1 m)	0.09	0.59	0.014	0.016	0.13	−15.1	−48.9			
OSW1 (2 m)	0.12	0.56	0.014	0.018	0.095	−15.2	−49.2			
OSW1 (4 m)	0.13	0.55	0.013	0.035	0.071	−15.1	−50.3			
OSW1 (6 m)	0.15	0.58	0.014	0.042	0.056	−15.9	−52.1			
OSW1 (8 m)	0.16	0.62	0.015	0.095	0.011	−16.6	−53.6			
OSW1 (10 m)	0.16	0.59	0.014	0.21	0	−18.2	−60.5			
OSW1 (12 m)	0.18	0.63	0.015	0.28	0	−19.1	−61.3			
OSW1 (14 m)	0.21	0.61	0.015	0.35	0	−19.5	−61.1			
OSW1 (16 m)	0.23	0.58	0.014	0.56	0	−19.6	−63.4			
OSW2	0.05	0.61	0.015	0.019	0.17	−15.1	−45.0	0.135	13.1	16.8

Similar to surface waters, the dissolved gas chemistry along the depth profiles of the OMW1, OMW2 and OSW1 sites was dominated by N_2. However, both CH_4 and CO_2 concentrations showed an increasing trend along the water column at Massaciuccoli Lake

and Cava Sisa. The dissolved CO_2 concentration at Massaciuccoli Lake increased from 0.02 mmol/L at the water–atmosphere interface to 0.08 (OMW1) and 0.10 (OMW2) mmol/L in the bottom waters, whereas those of CH_4 increased ca. 2.5 times, i.e., from 0.0035 and 0.0031 mmol/L to 0.0088 and 0.0078 mmol/L in OMW1 and OMW2, respectively. At Cava Sisa, the increase in CO_2 and CH_4 concentrations with depth were up to one and two orders of magnitude from the surface (0.07 and 0.0087 mmol/L, respectively) to the bottom (0.23 and 0.56 mmol/L), respectively, with CH_4 becoming the second most abundant gas at ≥8 m depth. The O_2 concentrations showed an opposite trend with respect to CO_2 and CH_4, progressively decreasing with depth; at OSW, hypoxic conditions were found below 2 m depth, whereas no detectable dissolved O_2 was measured at ≥10 m depth (Table 4). The $\delta^{13}C$-CO_2 and $\delta^{13}C$-CH_4 values were relatively stable along the water column at Massaciuccoli Lake, with an overall decrease of ≤0.2 and ≤4.6‰ vs. V-PDB, respectively (Table 4). Conversely, a larger enrichment in lighter carbon isotopes was observed at OSW1, with $\delta^{13}C$-CO_2 and $\delta^{13}C$-CH_4 values varying from −14.6 and −43.7‰ vs. V-PDB, respectively, in surface waters to −19.6 and −63.4‰ vs. V-PDB, respectively, in bottom waters (Table 4).

3.4. CH_4 and CO_2 Diffusive Fluxes at Massaciuccoli Lake System

The CH_4 and CO_2 diffusive fluxes at the water–air interface calculated according to the TBL model are reported in Table 4. The ΦCH_4 values were comprised between 0.02 (OMW1 and OMW2) and 0.172 (LSW5) g CH_4 m^{-2} day^{-1}, although a particularly high value was recorded at LSW7, i.e., 1.61 g CH_4 m^{-2} day^{-1} (Table 4), which was also characterized by the highest CO_2 diffusive flux, i.e., 43.9 g CO_2 m^{-2} day^{-1}. On average, the LSW sites were characterized by the highest ΦCH_4 and ΦCO_2 values. Overall, ΦCO_2 values were ≥0.50 g CO_2 m^{-2} day^{-1}, although negative ΦCO_2 values were recorded for SPW, TCW4, ECW8 and OMW (from −3.49 to −0.03 g CO_2 m^{-2} day^{-1}). The resulting ΦCO_{2eq} values varied from −2.33 (TCW4) to 89 (LSW7) g CO_{2eq} m^{-2} day^{-1} (Table 4).

4. Discussion

4.1. CH_4 Emission Drivers at Porta Lake

The chemical composition of Porta Lake waters was strictly controlled by the Ca^{2+}-SO_4^{2-} springs that feed the lake, although a further shallow water source was possibly affecting those waters showing a HCO_3^- composition (Table 1). Seasonal variations in the lake water level were found, associated with changes in TDS and Eh values. The Eh values were relatively low, especially in summer, testifying of the presence of reducing conditions related to organic matter accumulation at the lake bottom and associated decomposition and mineralization processes. Accordingly, the dissolved O_2 concentrations were lower with respect to those expected for surface waters in equilibrium with air (Table 2), with the strongest O_2 depletion observed where the lake depth was relatively low (Figure 2a). These sites were also characterized by high concentrations of NH_4^+ and CH_4 (Tables 1 and 2) supplied by microbial activity in anoxic bottom sediments. It is well-known that CH_4 production under anoxic conditions may occur through two distinct pathways, i.e., acetoclastic methanogenesis and hydrogenotrophic methanogenesis, depending on the degradability of organic matter, e.g., [70–73]. The former, in which acetate serves as substrate, is considered to be more common in aquatic environments with large availability of labile organic matter; on the other hand, hydrogenotrophic methanogenesis, involving H_2 as electron acceptor, relies on more refractory organic matter. The two pathways produce distinct stable carbon isotopic signatures of CH_4, leading to $\delta^{13}C$-CH_4 values varying from −110 and −60‰ vs. V-PDB in the case of hydrogenotrophy and from −60 to −50‰ vs. V-PDB in the case of acetoclasty, e.g., [72,74,75]. As the water column depth decreased, CH_4 showed a progressive ^{12}C-enrichment, as expected for a microbial CH_4 production (Figure 2b), pointing to an isotope signature of CH_4 from methanogenesis around −60‰ vs. V-PDB, suggesting a prominent contribution from acetoclasty. Presumably, the presence of widespread reeds affected by RDBS at Porta Lake might play a significant role in enhancing

CH_4 production and, hence, its release to the atmosphere, by providing a higher organic matter accumulation rate, making more labile carbon substrates available for methanogenesis, e.g., [29,76–78]. These findings were in agreement with previous evidence that higher CH_4 ebullition rates in northern temperate lakes were predominantly supported by acetoclastic methanogenesis [79]. The large availability of autochthonous organic matter, providing abundant substrate for microbial activity, likely limited the competition between methanogenesis and sulfate reduction [80–82].

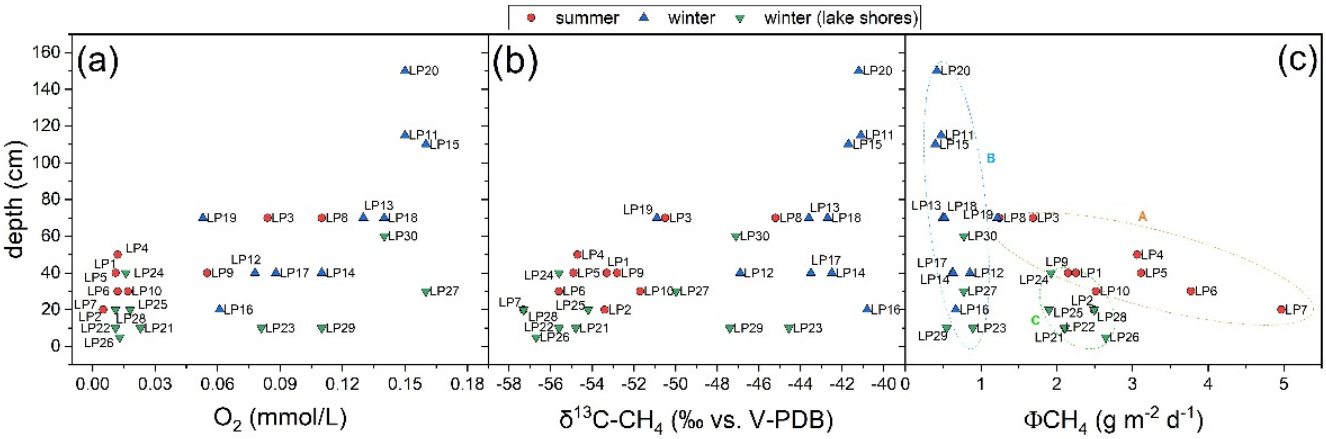

Figure 2. Water column depth (in cm) vs. (**a**) O_2 (in mmol/L), (**b**) δ^{13}C-CH_4 (in‰ vs. V-PDB) and (**c**) ΦCH_4 (in g m^{-2} day^{-1}) binary diagrams for samples collected from Porta Lake. Symbols as in Figure 1a. In (**c**), the dashed contour lines highlight the trends (A, B and C) described in detail in the text.

On the other hand, the overall decrease in ΦCH_4 values at increasing water column depth (Figure 2c) was likely related to more efficient surface water mixing and/or stratification processes in open waters, testified by higher O_2 contents (Figure 2a), resulting in more efficiency of oxidation processes affecting CH_4 slowly diffusing from the lake bottom towards the water–atmosphere interface. Accordingly, the increase in δ^{13}C-CH_4 values at decreasing dissolved CH_4 contents in surface waters (Figure 3) can adequately be described by a Rayleigh-type fractionation process (Figure 3), as follows:

$$\delta^{13}C - CH_{4_residual} = \left[\left(\delta^{13}C - CH_{4_{initial}} + 1000\right) \times f^{\frac{-\varepsilon_{CH_4-CO_2}}{1000}}\right] - 1000 \quad (7)$$

where $\delta^{13}C\text{-}CH_{4_initial}$ and $\delta^{13}C\text{-}CH_{4_residual}$ are the isotopic signatures of initial CH_4 (−60‰ vs. V-PDB) and residual CH_4 after oxidation, f is the fraction of residual CH_4 and $\varepsilon_{CH_4-CO_2}$is the fractionation factor for CH_4 oxidation to CO_2 during methanotrophy. The best fit of the data was obtained with a $\varepsilon_{CH_4-CO_2}$ value of about 8, in line with the values expected for carbon fractionation factors related to CH_4 oxidation (<10 [74]). Although this evidence confirmed the relevance of water column depth in controlling the CH_4 emissions within the wetland, which showed a variation range of one order of magnitude, different trends were observed in ΦCH_4 values (Figure 2c), as detailed below. The data registered in summer displayed a higher increase in CH_4 diffusive fluxes as the water column depth decreased (trend A) with respect to winter data. Such seasonal variation in the measured CH_4 diffusive fluxes was to be ascribed to the higher temperatures recorded in summer, which are expected to accelerate methane production rate from sediments, e.g., [83] and references therein. On the other hand, winter data showed two distinct behaviors: trends B and C in Figure 2c, with those samples collected from sites located close to the lake shores and in the reeds being characterized by higher ΦCH_4 values with respect to other sites of similar depth. Such behavior might be related to the diverse hydrological regimes encountered within the lake, with higher ΦCH_4 values where dense riparian reeds sheltering the lake waters from winds hinder mixing and oxygenation processes and produce more

stagnant waters (trend C), as testified by the lower O_2 contents (Figure 2a) with respect to open waters (trend B; Figure 2c). Moreover, the sites displaying anomalous ΦCH_4 values (trend C) were located in areas characterized by visible retreat of reed beds (Figure 1a). Accordingly, Sorrell et al. [76] demonstrated that methanogenesis rates in die-back sites were higher than those in the surrounding healthy reeds, suggesting that RDBS-affected wetlands might be intense sources of CH_4. This hypothesis was also supported by the data obtained at Porta Lake in summer, which displayed the highest ΦCH_4 values in sites of dying back reeds (LP6 and LP7). Even though their role in regulating lake CH_4 emissions has been long debated, e.g., [84,85] and references therein, macrophytes were recognized as important sources of autochthonous labile carbon in aquatic environments, e.g., [77] and the macrophyte detritus was demonstrated to improve CH_4 production in anoxic sediments, e.g., [78]. Similarly, Emilson et al. [86] found that macrophyte litter determined a $\geq$400 times higher CH_4 production than terrestrial sources.

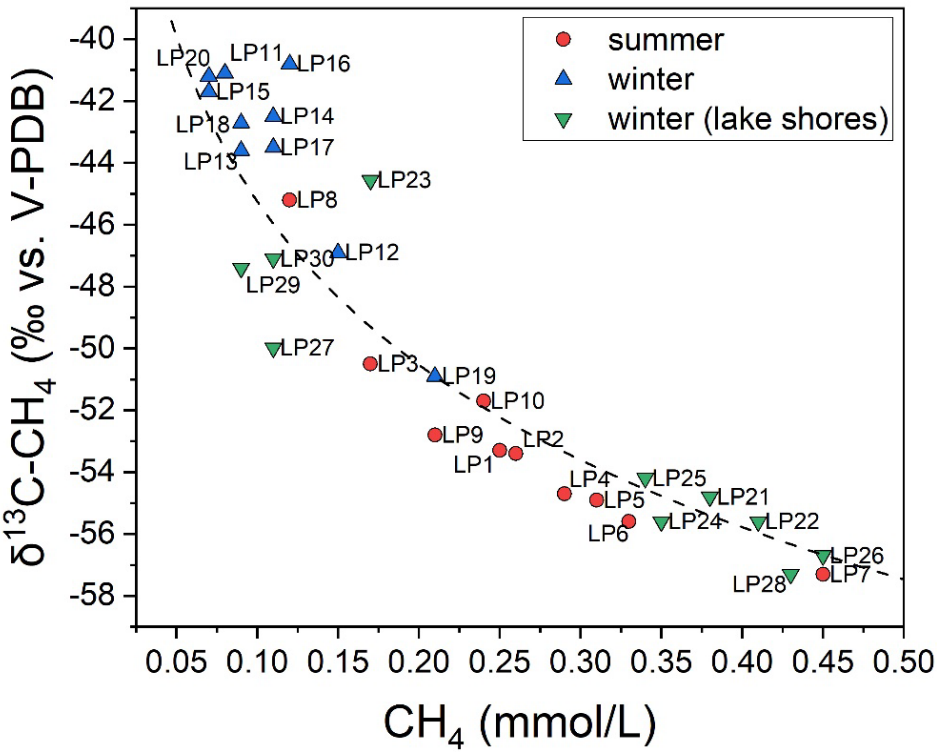

Figure 3. $\delta^{13}C$-CH_4 (in‰ vs. V-PDB) vs. CH_4 (in mmol/L) binary diagram for samples collected in summer and winter from Porta Lake. Symbols as in Figure 1a. The Rayleigh fractionation evolution curve for CH_4 oxidation to CO_2 related to methanotrophic activity, as described in the text, is also reported (dashed line).

As shown in Figure 4, where the CH_4 diffusive fluxes measured at Porta Lake were compared with those recently compiled from literature data by Rosentreter et al. [17], the ΦCH_4 values from the present study largely exceeded the average value reported for diffusive fluxes from diverse aquatic ecosystems and were anomalously high with respect to the range reported in literature for lakes and reservoirs. On average, the ΦCH_4 values at Porta Lake even exceeded those exceptionally high values recently reported for a tropical lake in Kenya (ca. 0.97 g CH_4 m^{-2} day^{-1} [24]).

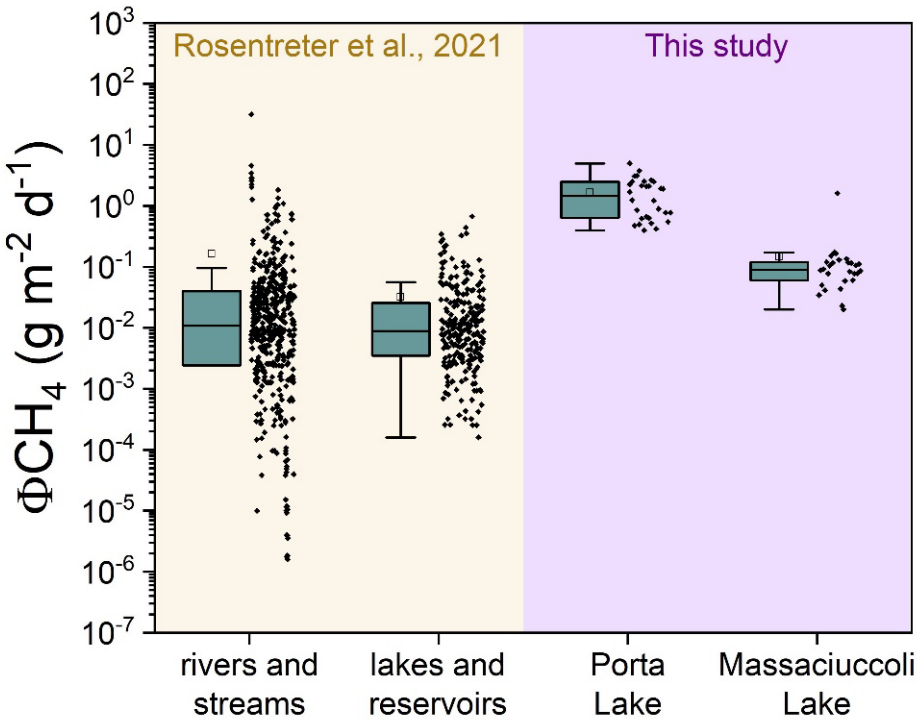

Figure 4. ΦCH_4 (in g m^{-2} day^{-1}) values from different aquatic systems (rivers and streams, lakes and reservoirs) as reported in Rosentreter et al. [17] compared with those measured at Porta and Massaciuccoli Lakes (present study).

The high CH_4 fluxes at Porta Lake were also associated with high ΦCO_2 values (Figure 5a); as the concentration of dissolved CO_2 increased, the $\delta^{13}C$-CO_2 values decreased, approaching the typical isotopic signature from degradation of organic matter [56] and references therein (Table 2). The resulting ΦCO_{2eq} values testified that Porta Lake was a significant source of GHGs to the atmosphere.

4.2. CH_4 Emission Drivers at Massaciuccoli Lake System

The chemical features of the waters collected from Massaciuccoli Lake system resulted from multiple factors, including: (i) chemical variability of the feeding waters, (ii) direct mixing with seawater, (iii) anthropogenic inputs from urban, agricultural and industrial areas and (iv) biogeochemical processes exacerbated by eutrophication, e.g., [47,48,87]. The water isotope signature evidenced that most waters were significantly affected by isotope fractionation due to evaporation processes, except those less exposed to solar radiation, i.e., from the Case Rosse spring (SPW) and most tributary channels (TCW) (Figure 6).

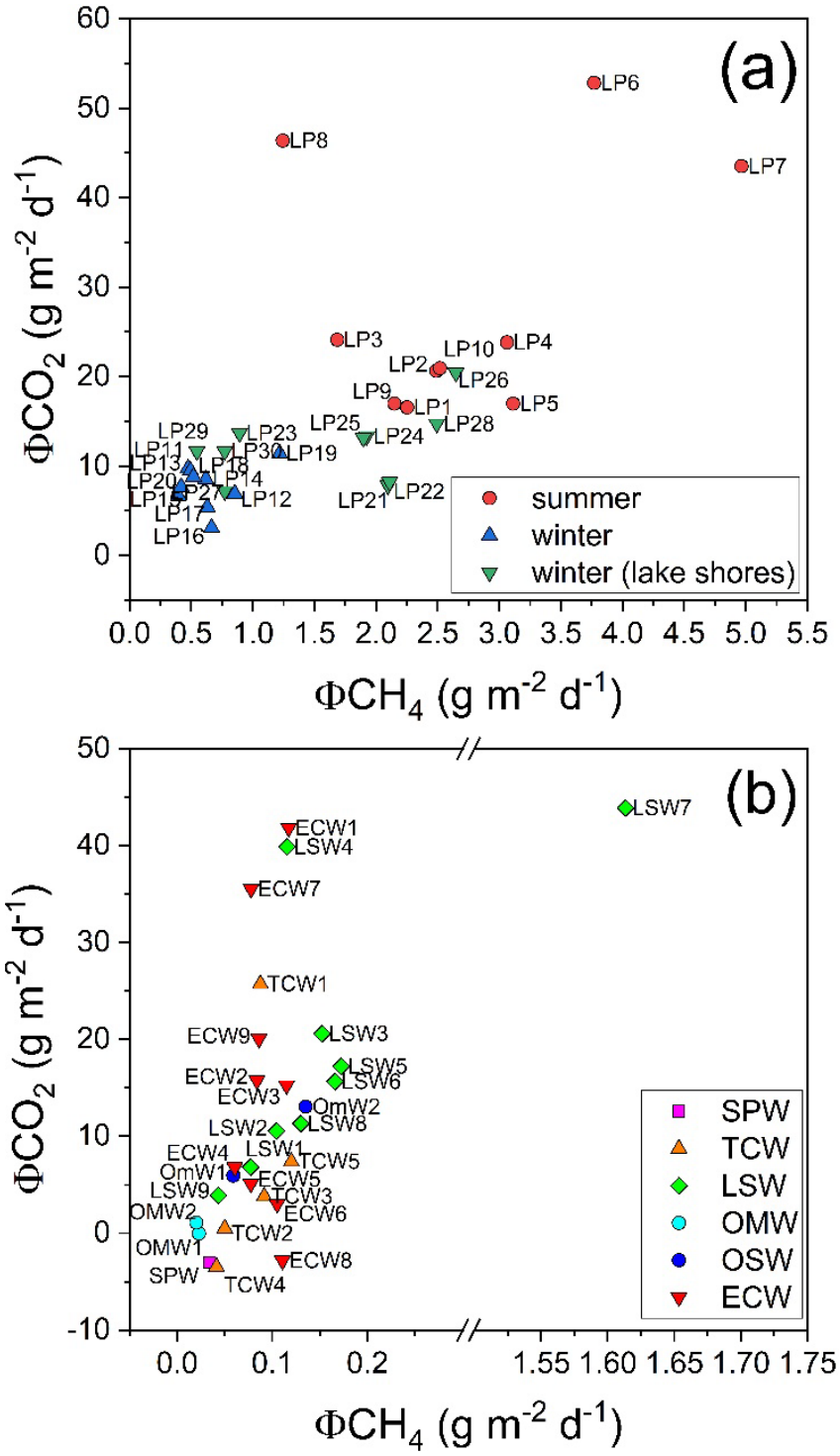

Figure 5. ΦCO_2 vs. ΦCH_4 (in g m^{-2} day^{-1}) binary diagrams for samples collected from (**a**) Porta Lake, with symbols as in Figure 1a) and (**b**) Massaciuccoli Lake system. Symbols as in Figure 1b.

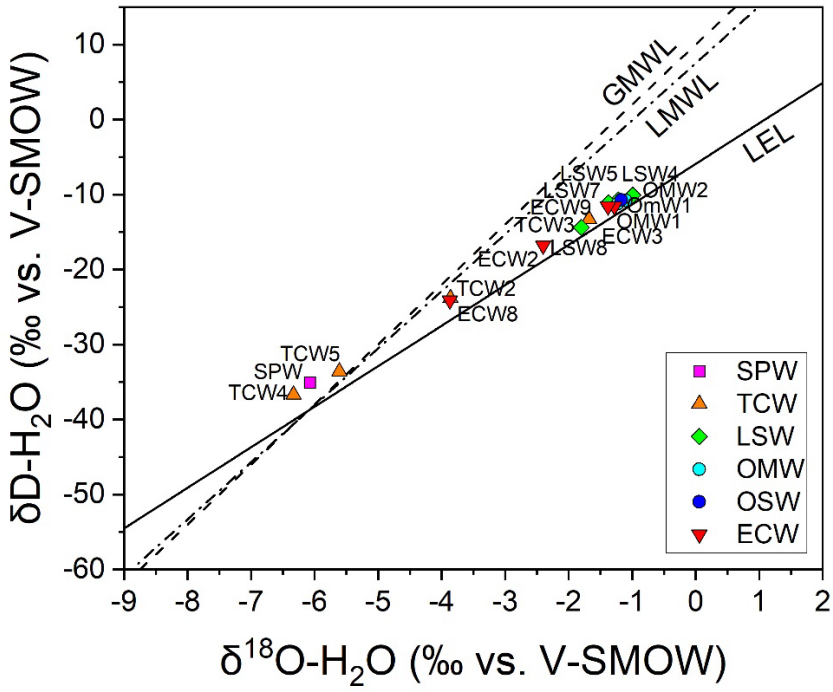

Figure 6. δD-H_2O vs. δ^{18}O-H_2O (in‰ vs. V-SMOW) binary diagram for water samples collected from Massaciuccoli Lake. Symbols as in Figure 1b. Global meteoric water line (GMWL: $\delta D = 8 \times \delta^{18}O + 10$ [88]), local meteoric water line (LMWL: $\delta D = 7.6 \times \delta^{18}O + 7.5$ [47]) and local evaporation line (LEL: $\delta D = 5.4 \times \delta^{18}O - 5.9$ [47]).

The water springs in the area included both Ca^{2+}-HCO_3^- waters, e.g., the SPW sample collected from the Case Rosse spring, and Ca^{2+}-SO_4^{2-} waters, such as the one (named Villa Spinola), which feeds the Quiesa channel (TCW4). However, the chemical composition of the waters collected from Massaciuccoli Lake system was largely dominated by Na^+ and Cl^-. The Na^+/Cl^- mass ratios ranged from 0.50 to 0.69, suggesting the direct influence of seawater (Na^+/Cl^- mass ratio = 0.56) in agreement with Baneschi [47]). Accordingly, the TDS values progressively increased approaching the coastline, the lowest values being measured in the TCW samples and the highest ones in those from ECW, including the Burlamacca canal. Coherently, the average Cl^-/Br^- mass ratio value in the collected samples (308) was close to that of seawater (292). Nevertheless, higher Cl^-/Br^- mass ratio values (≥384) were occasionally observed, especially in samples from Cava Sisa (LSW1, LSW2, LSW3, LSW4 and OSW2) and TCW1, likely related to anthropogenic inputs and/or Br assimilation processes by green plants and phytoplankton [47] and references therein. In fact, biogeochemical processes shaped the chemical features of waters and dissolved gases within the lake, as observed along the OSW1 vertical profile where decomposition processes at the lake bottom produced a chemocline at around 10 m depth, separating the anoxic and NH_4-rich waters from the shallow levels. The variations of the δ^{13}C-TDIC values along the water column supported the occurrence of decomposition processes at the lake bottom, with a ^{12}C-enriched TDIC, whereas enrichments in the heavier ^{13}C isotope were observed in shallow waters due to photosynthetic activity and exchanges with the atmosphere. Coherently, the δ^{13}C-CO_2 values in shallow waters along the OSW1 vertical profile were characterized by a ^{13}C-enrichment with respect to bottom waters. Methanogenesis occurring in bottom waters and lake sediments produced an increase in dissolved CH_4 concentrations enriched in the lighter carbon isotope downwards the water column. Different from Porta Lake, no clear relationship was recognized between dissolved O_2 contents and water column depth (Figure 7a), likely due to the wide variability of physicochemical features encountered in Massaciuccoli Lake system, suggesting that depth was not sufficient to predict the mixing degree of the water column. Similarly, both

δ^{13}C-CH_4 values and CH_4 diffusive fluxes at the water–air interface varied independently from the water column depth (Figure 7b,c), confirming that this physical environmental feature alone was not informative of the extent of CH_4 release to the atmosphere. As observed at Porta Lake, the CH_4 emissions were expected to be controlled by both (i) water mixing/stratification, regulating the oxidation of CH_4 along its ascent towards the water–atmosphere interface, and (ii) rate of microbial activity, determining the extent of CH_4 production mostly occurring within the bottom sediments. In the case of Massaciuccoli Lake system, the former was likely controlled by morphological settings rather than water depth, whereas the latter was likely modulated by several factors, including quality and quantity of available organic matter. The measured δ^{13}C-CH_4 values pointed to ca. −65‰ vs. V-PDB as the CH_4 contents increased (Figure 8), suggesting the involvement of largely and readily available organic substrates for acetoclastic methanogenesis. Notably, the highest ΦCH_4 value, up to two orders of magnitude higher than those measured in the other sites, was recorded at LSW7, i.e., a sampling site located within an area largely covered by reed beds [50] (Figure 1b), confirming the relevant dual role of reed beds in (i) providing labile organic matter enhancing CH_4 production while (ii) sheltering winds and hindering water oxygenation. Notably, the ΦCH_4 values at Massaciuccoli Lake were within the range reported in literature for lakes and reservoirs (Figure 4), with the sole exception of LSW7.

On the other hand, whilst the increase in the δ^{13}C-CH_4 values at decreasing dissolved CH_4 contents (Figure 8) was in agreement with a Rayleigh-type fractionation process (Equation (7)), with a $\varepsilon_{CH_4-CO_2}$ value of about 5, similar to that observed by Whiticar [74] based on field observations, the fractionation factor (ε_C) between CO_2 and CH_4 tended to ca. 45‰ vs. V-PDB (Table 4) at decreasing δ^{13}C-CH_4 values, in agreement with the ε_C values expected for freshwater environments dominated by acetate fermentation [74].

The ΦCO_2 values at Massaciuccoli Lake system largely varied from negative values up to 43.9 g m^{-2} day^{-1}, the highest values being observed within the reed beds (LSW7). Overall, high CH_4 fluxes were associated with high ΦCO_2 values (Figure 5b), confirming a strict relationship among the diffusive emissions of these two GHGs from waterbodies and their common origin related to the degradation of organic matter, as supported by the measured δ^{13}C-CO_2 values (Table 4). Although Massaciuccoli Lake system displayed lower ΦCO_{2eq} values with respect to those of Porta Lake, with local areas where photosynthetic activity produced negative fluxes (i.e., CO_2 uptake from the atmosphere), relevant hot spots of intense GHGs emissions were recognized (LSW7).

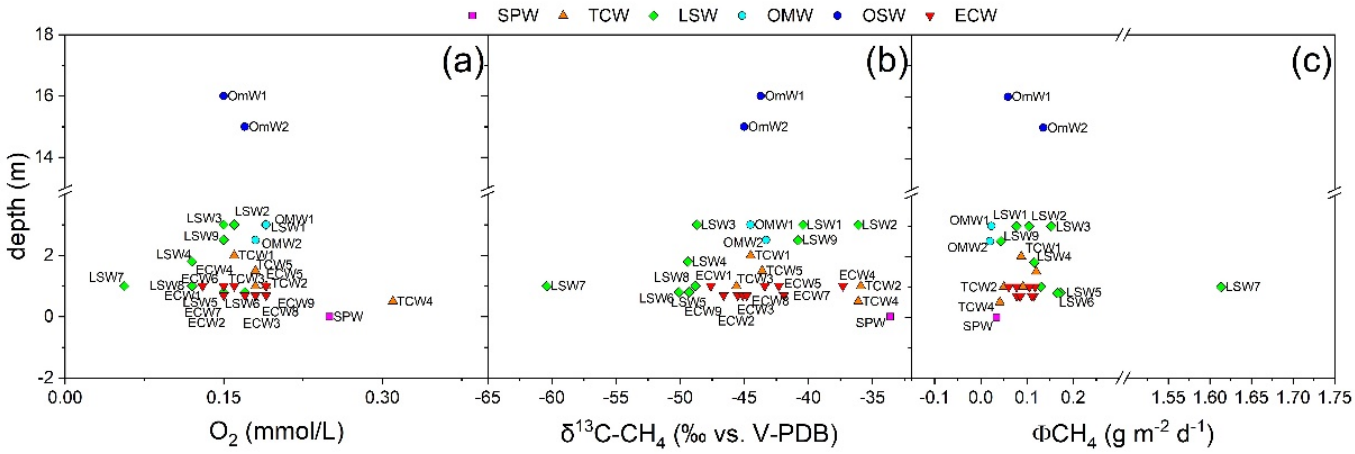

Figure 7. Water column depth (in cm) vs. (**a**) O_2 (in mmol/L), (**b**) δ^{13}C-CH_4 (in‰ vs. V-PDB) and (**c**) ΦCH_4 (in g m^{-2} day^{-1}) binary diagrams for samples collected from Massaciuccoli Lake. Symbols as in Figure 1b.

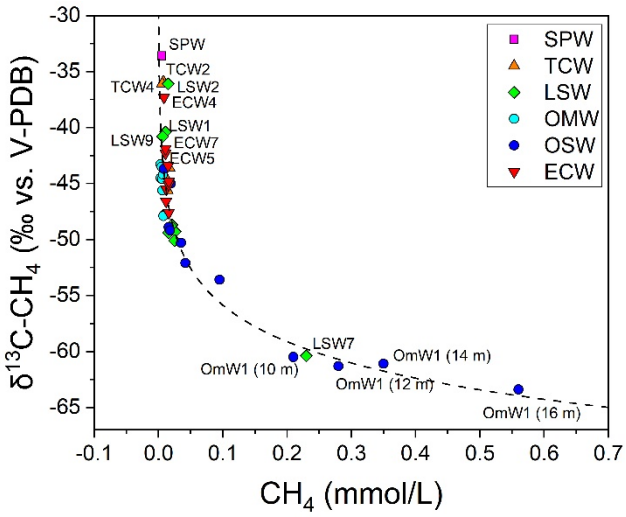

Figure 8. δ^{13}C-CH_4 (in‰ vs. V-PDB) vs. CH_4 (in mmol/L) binary diagram for samples collected from Massaciuccoli Lake. Symbols as in Figure 1b. The Rayleigh fractionation evolution curve for CH_4 oxidation to CO_2 related to methanotrophic activity, as described in the text, is also reported (dashed line).

5. Conclusions

Porta and Massaciuccoli Lakes were recognized as net sources of CH_4 and CO_2 to the atmosphere, with measured CO_{2eq} emissions to the atmosphere up to 183 g CO_{2eq} m^{-2} day^{-1}. The magnitude of CH_4 diffusive emission at the water–air interface was strictly dependent on the balance between CH_4 production and consumption rates. Methane consumption, mostly due to aerobic methanotrophy, was influenced by dissolved O_2 contents, which, in turn, were related to the water column depth and stratification/mixing processes. The latter were likely governed by winds, lake morphology and vegetation, with reed beds acting as barriers to water movements and favoring the development of stagnant and hypoxic conditions in surface waters. Methane production rates were affected by both seasonal variations, due to the temperature dependence of microbial activity and quality and quantity of organic matter. In fact, evidence from both lakes suggested that the highest CH_4 diffusive fluxes were sustained by the presence of reed beds providing shelter from the wind and ensuring a large availability of labile organic matter. Accordingly, the ΦCH_4 values in sites proximal to reed beds were up to two orders of magnitude higher than those measured in open waters.

The results of this study highlighted that magnitude of CH_4 diffusive emissions across wetland systems is strongly site-dependent and shaped by local environmental conditions, which might highly be variable in both time and space. Hence, the sampling strategies, timing and site selection have to be carefully evaluated since they might largely affect the estimation of overall CH_4 diffusive emissions even within a single wetland system. Efforts to increase both spatial and temporal resolution of CH_4 diffusive flux measurements to evaluate the diverse environmental conditions characterizing wetland landscapes are to be considered. Promising opportunities are offered by integrating traditional CH_4 diffusive flux measurements with the deployment of low-cost CH_4 sensors in flux chambers [89].

Nevertheless, the CH_4 diffusive fluxes measured in this study, largely exceeding those reported in literature (Figure 4), indicate that a relevant portion of CH_4 emissions from surface aquatic systems at global scale is likely missing in carbon budgets, with relevant implications for Earth system and climate models. It is to be pointed out that the investigated sites did not include areas with higher density of reed beds where the ΦCH_4 values might be even greater. Moreover, the CH_4 emissions associated with plant litter in wetlands are expected to increase in the near future as a consequence of both eutrophication processes and climate change [3]. Moreover, the relationship between RDBS

and CH_4 diffusive fluxes is particularly alarming, considering that wetlands are among the most threatened ecosystems on Earth, drawing attention to the urgent need to protect and restore wetland ecological functioning.

Author Contributions: Conceptualization, S.V. and F.T.; methodology, S.V. and F.T.; formal analysis, S.V., F.C., M.L. and A.R.; investigation, S.V., F.C., M.L., A.R., F.T., J.C. and O.V.; resources, B.V.; data curation, F.T. and F.C.; writing—original draft preparation, S.V.; writing—review and editing, F.T., J.C., A.R., F.C. and O.V.; visualization, S.V.; supervision, B.V.; project administration, S.V. and O.V.; funding acquisition, O.V. All authors have read and agreed to the published version of the manuscript.

Funding: This research received no external funding.

Acknowledgments: The authors want to thank Gianluca Giannelli (WWF) for their support during sampling and measuring campaigns. This work was partly financially supported by an agreement between the Municipality of Montignoso and the Department of Earth Sciences, University of Florence (Resp. SV and OV) and the Laboratory of Fluid Geochemistry at the Department of Earth Sciences, University of Florence. Two anonymous reviewers are warmly thanked for their comments and useful suggestions that improved an early version of the manuscript.

Conflicts of Interest: The authors declare no conflict of interest.

References

1. Downing, J.A.; Prairie, Y.T.; Cole, J.J.; Duarte, C.M.; Tranvik, L.J.; Striegl, R.G.; McDowell, W.H.; Kortelainen, P.; Caraco, N.F.; Melack, J.M.; et al. The gobal abundance and size distribution of lakes, ponds, and impoundments. *Limnol. Oceanogr.* **2006**, *51*, 2388–2397. [CrossRef]
2. Ciężkowski, W.; Szporak-Wasilewska, S.; Kleniewska, M.; Jóźwiak, J.; Gnatowski, T.; Dąbrowski, P.; Góraj, M.; Szatyłowicz, J.; Ignar, S.; Chormański, J. Remotely sensed land surface temperature-based water stress index for wetland habitats. *Remote Sens.* **2020**, *12*, 631. [CrossRef]
3. Koffi, E.N.; Bergamaschi, P.; Alkama, R.; Cescatti, A. An observation-constrained assessment of the climate sensitivity and future trajectories of wetland methane emissions. *Sci. Adv.* **2020**, *6*, eaay4444. [CrossRef] [PubMed]
4. Salimi, S.; Almuktar, S.A.A.A.N.; Scholz, M. Impact of climate change on wetland ecosystems: A critical review of experimental wetlands. *J. Environ. Manag.* **2021**, *286*, 112160. [CrossRef] [PubMed]
5. Lal, R. Carbon sequestration. *Philos. Trans. R. Soc. Lond. B Biol. Sci.* **2008**, *363*, 815–830. [CrossRef]
6. Nellemann, C.; Corcoran, E.; Duarte, C.M.; Valdrés, L.; De Young, C.; Fonseca, L.; Grimsditch, G.; Blue Carbon. A rapid response assessment.United Nations Environment Programme, GRID-Arendal. 2009. Available online: www.grida.no (accessed on 21 October 2021).
7. Moomaw, W.R.; Chmura, G.L.; Davies, G.T.; Finlayson, C.M.; Middleton, B.A.; Natali, S.M.; Perry, J.E.; Roulet, N.; Sutton-Grier, A. Wetlands in a changing climate: Science, policy and management. *Wetlands* **2018**, *38*, 183–205. [CrossRef]
8. Beaulieu, J.J.; DelSontro, T.; Downing, J.A. Eutrophication will increase methane emissions from lakes and impoundments during the 21st century. *Nat. Commun.* **2019**, *10*, 1375. [CrossRef]
9. Limpert, K.E.; Carnell, P.E.; Trevathan-Tackett, S.M.; Macreadie, P.I. Reducing emissions from degraded floodplain wetlands. *Front. Environ. Sci.* **2020**, *8*, 8. [CrossRef]
10. Myhre, G.; Shindell, D.; Bréon, F.M.; Collins, W.; Fuglestvedt, J.; Huang, J.; Koch, D.; Lamarque, J.-F.; Lee, D.; Mendoza, B.; et al. Anthropogenic and Natural Radiative Forcing. In *Climate Change 2013: The Physical Science Basis. Contribution of Working Group I to the Fifth Assessment Report of the Intergovernmental Panel on Climate Change*; Stocker, T.F., Qin, D., Plattner, G.-K., Tignor, M., Allen, S.K., Boschung, J., Nauels, A., Xia, Y., Bex, V., Midgley, P.M., Eds.; Cambridge University Press: Cambridge, UK; New York, NY, USA, 2013.
11. Rigby, M.; Prinn, R.G.; Fraser, P.J.; Simmonds, P.G.; Langenfelds, R.L.; Huang, J.; Cunnold, D.M.; Steele, L.P.; Krummel, P.B.; Weiss, R.F.; et al. Renewed growth of atmospheric methane. *Geophys. Res. Lett.* **2008**, *35*, L22805. [CrossRef]
12. Dlugokencky, E.J.; Bruhwiler, L.; White, J.W.C.; Emmons, L.K.; Novelli, P.C.; Montzka, S.A.; Masarie, K.A.; Lang, P.M.; Crotwell, A.M.; Miller, J.B.; et al. Observational constraints on recent increases in the atmospheric CH_4 burden. *Geophys. Res. Lett.* **2009**, *36*, L18803. [CrossRef]
13. Dlugokencky, E. Trends in Atmospheric Methane. In *NOAA/GML*; 2021. Available online: https://gml.noaa.gov/ccgg/trends_ch4/ (accessed on 21 October 2021).
14. Nisbet, E.G.; Dlugokencky, E.J.; Manning, M.R.; Lowry, D.; Fisher, R.E.; France, J.L.; Michel, S.E.; Miller, J.B.; White, J.W.C.; Vaughn, B.; et al. Rising atmospheric methane: 2007–2014 growth and isotopic shift. *Glob. Biogeochem. Cycles* **2016**, *30*, 1356–1370. [CrossRef]

15. Nisbet, E.G.; Manning, M.R.; Dlugokencky, E.J.; Fisher, R.E.; Lowry, D.; Michel, S.E.; Lung Myhre, C.; Platt, S.M.; Allen, G.; Bousquet, P.; et al. Very strong atmospheric methane growth in the 4 years 2014–2014: Implications for the Paris Agreement. *Glob. Biogeochem. Cycles* **2019**, *33*, 318–342. [CrossRef]
16. Lan, X.; Basu, S.; Schwietzke, S.; Bruhwiler, L.M.P.; Dlugokencky, E.J.; Michel, S.E.; Sherwood, O.A.; Tans, P.P.; Thoning, K.; Etiope, G.; et al. Improved constraints on global methane emissions and sinks using δ^{13}C-CH_4. *Glob. Biogeochem. Cycles* **2021**, *35*, e2021GB007000. [CrossRef]
17. Rosentreter, J.A.; Borges, A.V.; Deemer, B.R.; Holgerson, M.A.; Liu, S.; Song, C.; Melack, J.; Raymond, P.A.; Duarte, C.M.; Allen, G.H.; et al. Half of global methane emissions come from highly variable aquatic ecosystem sources. *Nat. Geosci.* **2021**, *14*, 225–230. [CrossRef]
18. Carmichael, M.J.; Bernhardt, E.S.; Bräuer, S.L.; Smith, W.K. The role of vegetation in methane flux to the atmosphere: Should vegetation be included as a distinct category in the global methane budget? *Biogeochemistry* **2014**, *119*, 1–24. [CrossRef]
19. Waldo, N.B.; Hunt, B.K.; Fadely, E.C.; Moran, J.J.; Neumann, R.B. Plant root exudates increase methane emissions through direct and indirect pathways. *Biogeochemistry* **2019**, *145*, 213–234. [CrossRef]
20. Tang, K.W.; McGinnis, D.F.; Ionescu, D.; Grossart, H.P. Methane production in oxic lake waters potentially increases aquatic methane flux to air. *Environ. Sci. Technol. Lett.* **2016**, *3*, 227–233. [CrossRef]
21. Donis, D.; Flury, S.; Stöckli, A.; Spangenberg, J.E.; Vachon, D.; McGinnis, D.F. Full-scale evaluation of methane production under oxic conditions in a mesotrophic lake. *Nat. Commun.* **2017**, *8*, 1661. [CrossRef] [PubMed]
22. Tassi, F.; Cabassi, J.; Andrade, C.; Callieri, C.; Silva, C.; Viveiros, F.; Corno, G.; Vaselli, O.; Selmo, E.; Gallorini, A.; et al. Mechanisms regulating CO_2 and CH_4 dynamics in the Azorean volcanic lakes (São Miguel Island, Portugal). *J. Limnol.* **2018**, *77*, 483–504. [CrossRef]
23. Günthel, M.; Donis, D.; Kirillin, G.; Ionescu, D.; Bizic, M.; McGinnis, D.F.; Grossart, H.P.; Tang, K.W. Contribution of oxic methane production to surface methane emission in lakes and its global importance. *Nat. Commun.* **2019**, *10*, 5497. [CrossRef]
24. Fazi, S.; Amalfitano, S.; Venturi, S.; Pacini, N.; Vazquez, E.; Olaka, L.A.; Tassi, F.; Crognale, S.; Herzsprung, P.; Lechtenfeld, O.J.; et al. High concentrations of dissolved biogenic methane associated with cyanobacterial blooms in East African lake surface water. *Commun. Biol.* **2021**, *4*, 845. [CrossRef]
25. Sanches, L.F.; Guenet, B.; Marinho, C.C.; Barros, N.; de Assis Esteves, F. Global regulation of methane emission from natural lakes. *Sci. Rep.* **2019**, *9*, 255. [CrossRef] [PubMed]
26. Bastviken, D.; Cole, J.; Pace, M.; Tranvik, L. Methane emissions from lakes: Dependence of, GB lake characteristics, two regional assessments, and a global estimate. *Glob. Biogeochem. Cycles* **2004**, *18*, GB4009. [CrossRef]
27. Hofmann, H. Spatiotemporal distribution patterns of dissolved methane in lakes: How accurate are the current estimations of the diffusive flux path? *Geophys. Res. Lett.* **2013**, *40*, 2779–2784. [CrossRef]
28. Attermeyer, K.; Flury, S.; Jayakumar, R.; Fiener, P.; Steger, K.; Arya, V.; Wilken, F.; van Geldern, R.; Premke, K. Invasive floating macrophytes reduce greenhouse gas emissions from a small tropical lake. *Sci. Rep.* **2016**, *6*, 20424. [CrossRef]
29. dos Santos Fonseca, A.L.; Cardoso Marinho, C.; de Assis Esteves, F. Floating aquatic macrophytes decrease the methane concentration in the water column of a tropical coastal lagoon: Implications for methane oxidation and emission. *Braz. Arch. Biol. Technol.* **2017**, *60*, e17160381.
30. Milberg, P.; Törnqvist, L.; Westerberg, L.M.; Bastviken, D. Temporal variations in methane emissions from emergent aquatic macrophytes in two boreonemoral lakes. *AoB Plants* **2017**, *9*, plx029. [CrossRef] [PubMed]
31. Jeffrey, L.C.; Maher, D.T.; Johnston, S.G.; Kelaher, B.P.; Steven, A.; Tait, D.R. Wetland methane emissions dominated by plant-mediated fluxes: Contrasting emissions pathways and seasons within a shallow freshwater subtropical wetland. *Limnol. Oceanogr.* **2019**, *64*, 1895–1912. [CrossRef]
32. Bansal, S.; Johnson, O.F.; Meier, J.; Zhu, X. Vegetation affects timing and location of wetland methane emissions. *J. Geophys. Res. Biogeosci.* **2020**, *125*, e2020JG005777. [CrossRef]
33. van den Berg, M.; Ingwersen, J.; Lamers, M.; Streck, T. The role of *Phragmites* in the CH_4 and CO_2 fluxes in a minerotrophic peatland in southwest Germany. *Biogeosciences* **2016**, *13*, 6107–6119. [CrossRef]
34. van den Berg, M.; van den Elzen, E.; Ingwersen, J.; Kosten, S.; Lamers, L.P.M.; Streck, T. Contribution of plant-induced pressurized flow to CH_4 emission from a *Phragmites* fen. *Sci. Rep.* **2020**, *10*, 12304. [CrossRef]
35. Kim, J.; Chaudhary, D.R.; Lee, J.; Byun, C.; Byun, C.; Ding, W.; Kwon, B.O.; Khim, J.S.; Kang, H. Microbial mechanism for enhanced methane emission in deep soil layer of *Phragmites*-introduced tidal marsh. *Environ. Int.* **2020**, *134*, 105251. [CrossRef] [PubMed]
36. Deemer, B.R.; Holgerson, M.A. Drivers of methane flux differ between lakes and reservoirs, complicating global upscaling efforts. *J. Geophys. Res. Biogeosci.* **2021**, *126*, e2019JG005600. [CrossRef]
37. Vaselli, O.; Venturi, S.; Cabassi, J.; Lazzaroni, M.; Randazzo, A.; Tassi, F.; Capecchiacci, F.; Giannini, L.; Vietina, B. *Monitoraggio di parametri fisico-chimici di acque e sedimenti e modello idrogeochimico del Lago di Porta (Massa-Carrara, Toscana)*; Technical Report of the Department of Earth Sciences, University of Florence, for the Municipality of Montignoso (Massa-Carrara, Tuscany); University of Florence: Florence, Italy, 2021.
38. Ganesan, A.L.; Stell, A.C.; Gedney, N.; Comyn-Platt, E.; Hayman, G.; Rigby, M.; Poulter, B.; Hornibrook, E.R.C. Spatially resolved isotopic source signatures of wetland methane emissions. *Geophys. Res. Lett.* **2018**, *45*, 3737–3745. [CrossRef]

39. Da Prato, S.; Baneschi, I. The coastal wetland systems of northern Tuscany: Massaciuccoli Lake and ex Porta Lake. State of knowledge and new opportunities for multidisciplinary approach. *Ital. J. Groundw.* **2020**, *9*, 51–54. [CrossRef]
40. Costantini, E.A.C.; Barbetti, R.; Fantappiè, M.; L'Abate, G.; Lorenzetti, R.; Magini, S. Pedodiversity. In *The Soils of Italy*; Costantini, E.A.C., Dazzi, C., Eds.; Springer: Dordrecht, The Netherlands, 2013; pp. 105–178.
41. Turba, C.A.; Lunardini, F. *Studio geologico, geomorfologico ed idrogeologico. A.I.A. Progetto di completamento della discarica per rifiuti speciali non pericolosi sita in Loc. Porta*; Ambiente Apuane S.p.A.: Massa Carrara, Italy, 2011; p. 238.
42. van der Putten, W.H. Assessing ecological change in European wetlands: How to know what parameters should be monitored to evaluate the die-back of common reed (Phragmites australis)? *Stapfia* **1994**, *31*, 61–68.
43. van der Putten, W.H. Die-back of *Phragmites australis* in European wetlands: An overview of the European Research Programme on reed die-back and progression (1993–1994). *Aquat. Biol.* **1997**, *59*, 267–275. [CrossRef]
44. Gigante, D.; Venanzoni, R.; Zuccarello, V. Reed die-back in southern Europe? A case study from Central Italy. *C. R. Biol.* **2011**, *334*, 327–336. [CrossRef] [PubMed]
45. Lastrucci, L.; Gigante, D.; Vaselli, O.; Nisi, B.; Viciani, D.; Reale, L.; Coppi, A.; Fazzi, V.; Bonari, G.; Angiolini, C. Sediment chemistry and flooding exposure: A fatal cocktail for *Phragmites australis* in the Mediterranean basin? *Ann. Limnol. – Int. J. Limnol.* **2016**, *52*, 365–377. [CrossRef]
46. Baldaccini, G.N. Zone umide: Dal degrado al recupero ecologico. Il caso del lago di Massaciuccoli (Toscana nord-occidentale). *Biol. Ambient.* **2018**, *32*, 85–98.
47. Baneschi, I. Geochemical and Environmental Study of a Coastal Ecosystem: Massaciuccoli Lake (Northern Tuscany, Italy). Ph.D. Thesis, Department of Environmental Sciences, University Cà Foscari of Venice, Venice, Italy, 2007.
48. Ciurli, A.; Zuccari, P.; Alpi, A. Growth and nutrient absorption of two submerged aquatic macrophytes in mesocosms, for reinsertion in a eutrophicated shallow lake. *Wetl. Ecol. Manag.* **2009**, *17*, 107–115. [CrossRef]
49. Zuccarini, P.; Ciurli, A.; Alpi, A. Implications for shallow lake manipulation: Results of aquaria and enclosure experiments manipulating macrophytes, zooplankton and fish. *Appl. Ecol. Environ. Res.* **2011**, *9*, 123–140. [CrossRef]
50. Viciani, D.; Dell'Olmo, L.; Vicenti, C.; Lastrucci, L. Natura 2000 protected habitats, Massaciuccoli Lake (northern Tuscany, Italy). *J. Maps* **2017**, *13*, 219–226. [CrossRef]
51. Caliro, S.; Panichi, C.; Stanzione, D. Variation in the total dissolved carbon isotope composition of thermal waters of the Island of Ischia (Italy) and its implications for volcanic surveillance. *J. Volcanol. Geotherm. Res.* **1999**, *90*, 219–240. [CrossRef]
52. Tassi, F.; Vaselli, O.; Luchetti, G.; Montegrossi, G.; Minissale, A. *Metodo per la determinazione dei gas disciolti in acque naturali*; Int. Rep.; CNR-IGG: Florence, Italy, 2008; p. 11.
53. Tassi, F.; Vaselli, O.; Tedesco, D.; Montegrossi, G.; Darrah, T.; Cuoco, E.; Mapendano, M.Y.; Poreda, R.; Delgado Huertas, A. Water and gas chemistry at Lake Kivu (DRC): Geochemical evidence of vertical and horizontal heterogeneities in a multi-basin structure. *Geochem. Geophys. Geosyst.* **2009**, *10*, Q02005. [CrossRef]
54. Tassi, F.; Fazi, S.; Rossetti, S.; Pratesi, P.; Ceccotti, M.; Cabassi, J.; Capecchiacci, F.; Venturi, S.; Vaselli, O. The biogeochemical vertical structure renders a meromictic volcanic lake a trap for geogenic CO_2 (Lake Averno, Italy). *PLoS ONE* **2018**, *13*, e0193914. [CrossRef] [PubMed]
55. Salata, G.G.; Roelke, L.A.; Cifuentes, L.A. A rapid and precise method for measuring stable carbon isotope ratios of dissolved inorganic carbon. *Mar. Chem.* **2000**, *69*, 153–161. [CrossRef]
56. Venturi, S.; Tassi, F.; Bicocchi, G.; Cabassi, J.; Capecchiacci, F.; Capasso, G.; Vaselli, O.; Ricci, A.; Grassa, F. Fractionation processes affecting the stable carbon isotope signature of thermal waters from hydrothermal/volcanic systems: The examples of Campi Flegrei and Volcano Island (southern Italy). *J. Volcanol. Geotherm. Res.* **2017**, *345*, 46–57. [CrossRef]
57. Chiodini, G. Gases dissolved in groundwaters: Analytical methods and examples of applications in central Italy. In Proceedings of the Rome Seminar on Environmental Geochemistry, Castelnuovo Di Porto, Rome, Italy, 22–26 May 1996; pp. 135–148.
58. Caliro, S.; Chiodini, G.; Avino, R.; Cardellini, C.; Frondini, F. Volcanic degassing at Somma-Vesuvio (Italy) inferred by chemical and isotopic signatures of groundwater. *Appl. Geochem.* **2005**, *20*, 1060–1076. [CrossRef]
59. Frondini, F.; Cardellini, C.; Caliro, S.; Chiodini, G.; Morgantini, N. Regional groundwater flow and interactions with deep fluids in western Apennine: The case of Narni-Amelia chain (Central Italy). *Geofluids* **2012**, *12*, 182–196. [CrossRef]
60. Zhang, J.; Quay, P.D.; Wilbur, D.O. Carbon isotope fractionation during gas-water exchange and dissolution of CO_2. *Geochim. Cosmochim. Acta* **1995**, *59*, 107–114. [CrossRef]
61. Liss, P.S.; Slater, P.G. Flux of Gases across the Air-Sea Interface. *Nature* **1974**, *247*, 181–184. [CrossRef]
62. Wanninkhof, R. Relationship between wind speed and gas exchange over the ocean revisited. *Limnol. Oceanogr. Methods* **2014**, *12*, 351–362. [CrossRef]
63. Crusius, J.; Wanninkhof, R. Gas transfer velocities measured at low wind speed over a lake. *Limnol. Oceanogr.* **2003**, *48*, 1010–1017. [CrossRef]
64. Nightingale, P.D.; Malin, G.; Law, C.S.; Watson, A.J.; Liss, P.S.; Liddicoat, M.I.; Boutin, J.; Upstill-Goddard, R.C. In situ evaluation of air-sea gas exchange parametrizations using novel conservative and volatile tracers. *Global Biogeochem. Cycles* **2000**, *14*, 373–387. [CrossRef]
65. Hoover, T.E.; Berkshire, D.C. Effects of hydration on carbon dioxide exchange across an air-water interface. *J. Geophys. Res.* **1969**, *74*, 456–464. [CrossRef]

66. Wanninkhof, R.; Knox, M. Chemical enhancement of CO_2 exchange in natural waters. *Limnol. Oceanogr.* **1996**, *41*, 689–697. [CrossRef]
67. Zeebe, R.E. On the molecular diffusion coefficients of dissolved CO, HCO_3^-, and CO_3^{2-} and their dependence on isotopic mass. *Geochim. Cosmochim. Acta* **2011**, *75*, 2483–2498. [CrossRef]
68. Johnson, K.S. Carbon dioxide hydration and dehydration kinetics in seawater. *Limnol. Oceanogr.* **1982**, *27*, 849–855. [CrossRef]
69. Clark, I. *Groundwater Geochemistry and Isotopes*; CRC Press: Boca Raton, FL, USA, 2015.
70. Deppenmeier, U.; Müller, V.; Gottschalk, G. Pathways of energy conservation in methanogenic archaea. *Arch. Microbiol.* **1996**, *165*, 149–163. [CrossRef]
71. Conrad, R. Importance of hydrogenotrophic, aceticlastic and methylotrophic methanogenesis for methane production in terrestrial, aquatic and other anoxic environments: A mini review. *Pedosphere* **2020**, *30*, 25–39. [CrossRef]
72. Gruca-Rokosz, R.; Szal, D.; Bartoszek, L.; Pękala, A. Isotopic evidence for vertical diversification of methane production pathways in freshwater sediments of Nielisz reservoir (Poland). *CATENA* **2020**, *195*, 104803. [CrossRef]
73. Praetzel, L.S.E.; Plenter, N.; Schilling, S.; Schmiedeskamp, M.; Broll, G.; Knorr, K.H. Organic matter and sediment properties determine in-lake variability of sediment CO_2 and CH_4 production and emissions of a small and shallow lake. *Biogeosciences* **2020**, *17*, 5057–5078. [CrossRef]
74. Whiticar, M.J. Carbon and hydrogen isotope systematics of bacterial formation and oxidation of methane. *Chem. Geol.* **1999**, *161*, 291–314. [CrossRef]
75. Conrad, R. Quantification of methanogenic pathways using stable carbon isotopic signatures: A review and a proposal. *Org. Geochem.* **2005**, *36*, 739–752. [CrossRef]
76. Sorrell, B.K.; Brix, H.; Schierup, H.H.; Lorenzen, B. Die-back of *Phragmites australis*: Influence on the distribution and rate of sediment methanogenesis. *Biogeochemistry* **1997**, *36*, 173–188. [CrossRef]
77. Reitsema, R.E.; Meire, P.; Schoelynck, J. The future of freshwater macrophytes in a changing world: Dissolved organic carbon quantity and quality and its interactions with macrophytes. *Front. Plant Sci.* **2018**, *9*, 629. [CrossRef]
78. Grasset, C.; Abril, G.; Mendonça, R.; Roland, F.; Sobek, S. The transformation of macrophyte-derived organic matter to methane relates to plant water and nutrient contents. *Limnol. Oceanogr.* **2019**, *64*, 1737–1749. [CrossRef] [PubMed]
79. Thottathil, S.D.; Prairie, Y.T. Coupling of stable carbon isotopic signature of methane and ebullitive fluxes in northern temperate lakes. *Sci. Total Environ.* **2021**, *777*, 146117. [CrossRef] [PubMed]
80. Egger, M.; Lenstra, W.; Jong, D.; Meysman, F.J.R.; Sapart, C.J.; van der Veen, C.; Röckmann, T.; Gonzalez, S.; Slomp, C.P. Rapid sediment accumulation results in high methane effluxes from coastal sediments. *PLoS ONE* **2016**, *11*, e0161609. [CrossRef]
81. Martins, P.D.; Hoyt, D.W.; Bansal, S.; Mills, C.T.; Tfaily, M.; Tangen, B.A.; Finocchiaro, R.G.; Johnston, M.D.; McAdams, B.C.; Solensky, M.J.; et al. Abundant carbon substrates drive extremely high sulfate reduction rates and methane fluxes in Prairie Pothole Wetlands. *Glob. Chang. Biol.* **2017**, *23*, 3107–3120. [CrossRef] [PubMed]
82. Sela-Adler, M.; Ronen, Z.; Herut, B.; Antler, G.; Vigderovich, H.; Eckert, W.; Sivan, O. Co-existence of methanogenesis and sulfate reduction with common substrates in sulfate-rich estuarine sediments. *Front. Microbiol.* **2017**, *8*, 766. [CrossRef] [PubMed]
83. Fuchs, A.; Lyautey, E.; Montuelle, B.; Casper, P. Effects of increasing temperatures on methane concentrations and methanogenesis during experimental incubation of sediments from oligotrophic and mesotrophic lakes. *J. Geophys. Res. Biogeosci.* **2016**, *121*, 1394–1406. [CrossRef]
84. Xing, Y.; Xie, P.; Yang, H.; Wu, A.; Ni, L. The change of gaseous carbon fluxes following the switch of dominant producers from macrophytes to algae in a shallow subtropical lake of China. *Atmos. Environ.* **2006**, *40*, 8034–8043. [CrossRef]
85. Zhang, M.; Xiao, Q.; Zhang, Z.; Gao, Y.; Zhao, J.; Pu, Y.; Wang, W.; Xiao, W.; Liu, S.; Lee, X. Methane flux dynamics in a submerged aquatic vegetation zone in a subtropical lake. *Sci. Total Environ.* **2019**, *672*, 400–409. [CrossRef]
86. Emilson, E.J.S.; Carson, M.A.; Yakimovich, K.M.; Osterholz, H.; Dittmar, T.; Gunn, J.M.; Mykytczuk, N.C.S.; Basiliko, N.; Tanentzap, A.J. Climate-driven shifts in sediment chemistry enhance methane production in northern lakes. *Nat. Commun.* **2018**, *9*, 1801. [CrossRef] [PubMed]
87. Chiellini, C.; Guglielminetti, L.; Sarrocco, S.; Ciurli, A. Isolation of four microalgal strains from the Lake Massaciuccoli: Screening of common pollutants tolerance pattern and perspectives for their use in biotechnological applications. *Front. Plant Sci.* **2020**, *11*, 607651. [CrossRef]
88. Craig, H. Isotopic variations in meteoric waters. *Science* **1961**, *133*, 1702–1703. [CrossRef]
89. Bastviken, D.; Nygren, J.; Schenk, J.; Parellada Massana, R.; Duc, N.T. Technical note: Facilitating the use of low-cost methane (CH_4) sensors in flux chambers—Calibration, data processing, and an open-source make-it-yourself logger. *Biogeosciences* **2020**, *17*, 3659–3667. [CrossRef]